NOAA Technical Report NESS 86

Statistical and Synoptic Evaluations of TIROS-N and NOAA-6 Retrievals

Washington, D.C.
October 1981

U.S. DEPARTMENT OF COMMERCE
National Oceanic and Atmospheric Administration
National Earth Satellite Service

NOAA TECHNICAL REPORTS

National Earth Satellite Service Series

The National Earth Satellite Service (NESS) is responsible for the establishment and operation of the environmental satellite systems of NOAA.

Publication of a report in NOAA Technical Report NESS series will not preclude later publication in an expanded or modified form in scientific journals. NESS series of NOAA Technical Reports is a continuation of, and retains the consecutive numbering sequence of, the former series, ESSA Technical Report National Environmental Satellite Center (NESC), and of the earlier series, Weather Bureau Meteorological Satellite Laboratory (MSL) Report. Reports 1 through 39 are listed in publication NESC 56 of this series.

Reports in the series are available from the National Technical Information Service (NTIS), U.S. Department of Commerce, Sills Bldg., 5285 Port Royal Road, Springfield, VA 22161, in paper copy or microfiche form. Order by accession number, when given, in parentheses. Beginning with 64, printed copies of the reports, if available, can be ordered through the Superintendent of Documents, U.S. Government Printing Office, Washington, DC 20402. Prices given on request from the Superintendent of Documents or NTIS.

ESSA Technical Reports

NESC 46 Monthly and Seasonal Mean Global Charts of Brightness From ESSA 3 and ESSA 5 Digitized Pictures, February 1967-February 1968. V. Ray Taylor and Jay S. Winston, November 1968, 9 pp. plus 17 charts. (PB-180-717)

NESC 47 A Polynomial Representation of Carbon Dioxide and Water Vapor Transmission. William L. Smith, February 1969 (reprinted April 1971), 20 pp. (PB-183-296)

NESC 48 Statistical Estimation of the Atmosphere's Geopotential Height Distribution From Satellite Radiation Measurements. William L. Smith, February 1969, 29 pp. (PB-183-297)

NESC 49 Synoptic/Dynamic Diagnosis of a Developing Low-Level Cyclone and Its Satellite-Viewed Cloud Patterns. Harold J. Brodrick and E. Paul McClain, May 1969, 26 pp. (PB-184-612)

NESC 50 Estimating Maximum Wind Speed of Tropical Storms From High Resolution Infrared Data. L. F. Hubert, A. Timchalk, and S. Fritz, May 1969, 33 pp. (PB-184-611)

NESC 51 Application of Meteorological Satellite Data in Analysis and Forecasting. Ralph K. Anderson, Jerome P. Ashman, Fred Bittner, Golden R. Farr, Edward W. Ferguson, Vincent J. Oliver, Arthur H. Smith, James F. W. Purdom, and Rance W. Skidmore, March 1974 (reprint and revision of NESC 51, September 1969, and inclusion of Supplement, November 1971, and Supplement 2, March 1973), pp. 1--6C-18 plus references.

NESC 52 Data Reduction Processes for Spinning Flat-Plate Satellite-Borne Radiometers. Torrence H. MacDonald, July 1970, 37 pp. (COM-71-00132)

NESC 53 Archiving and Climatological Applications of Meteorological Satellite Data. John A. Leese, Arthur L. Booth, and Frederick A. Godshall, July 1970, pp. 1-1--5-8 plus references and appendixes A through D. (COM-71-00076)

NESC 54 Estimating Cloud Amount and Height From Satellite Infrared Radiation Data. P. Krishna Rao, July 1970, 11 pp. (PB-194-685)

NESC 56 Time-Longitude Sections of Tropical Cloudiness (December 1966-November 1967). J. M. Wallace, July 1970, 37 pp. (COM-71-00131)

NOAA Technical Reports

NESS 55 The Use of Satellite-Observed Cloud Patterns in Northern Hemisphere 500-mb Numerical Analysis. Roland E. Nagle and Christopher M. Hayden, April 1971, 25 pp. plus appendixes A, B, and C. (COM-73-50262)

NESS 57 Table of Scattering Function of Infrared Radiation for Water Clouds. Giichi Yamamoto, Masayuki Tanaka, and Shoji Asano, April 1971, 8 pp. plus tables. (COM-71-50312)

NESS 58 The Airborne ITPR Brassboard Experiment. W. L. Smith, D. T. Hilleary, E. C. Baldwin, W. Jacob, H. Jacobowitz, G. Nelson, S. Soules, and D. Q. Wark, March 1972, 74 pp. (COM-72-10557)

NESS 59 Temperature Sounding From Satellites. S. Fritz, D. Q. Wark, H. E. Fleming, W. L. Smith, H. Jacobowitz, D. T. Hilleary, and J. C. Alishouse, July 1972, 49 pp. (COM-72-50963)

NESS 60 Satellite Measurements of Aerosol Backscattered Radiation From the Nimbus F Earth Radiation Budget Experiment. H. Jacobowitz, W. L. Smith, and A. J. Drummond, August 1972, 9 pp. (COM-72-51031)

(Continued on inside back cover)

NOAA Technical Report NESS 86

Statistical and Synoptic Evaluations of TIROS-N and NOAA-6 Retrievals

Harold J. Brodrick, Carmella Watkins,
and Arnold Gruber

Washington, D.C.
October 1981

U.S. DEPARTMENT OF COMMERCE
Malcolm Baldrige, Secretary
National Oceanic and Atmospheric Administration
John V. Byrne, Administrator
National Earth Satellite Service
David S. Johnson, Assistant Administrator for Satellites

STATISTICAL AND SYNOPTIC EVALUATIONS OF TIROS N AND NOAA 6 RETRIEVALS

Harold J. Brodrick, Carmella Watkins, and Arnold Gruber

National Oceanic and Atmospheric Administration
National Earth Satellite Service
Washington, D.C.

ABSTRACT. TIROS N and NOAA 6 temperature retrievals are evaluated using statistical parameters and synoptic case studies. A period from September 1979 through April 1980 is examined with the use of the root mean square (RMS) and mean difference between matched pairs of radiosonde and satellite derived layer mean temperatures. The monthly samples are divided according to retrieval method (clear, partly cloudy, and cloudy), and topography type (land or sea). The principal results show that the largest RMS differences occur in the layers near the Earth's surface and in the tropopause region, with the clear retrievals giving the smallest RMS differences and cloudy retrievals producing the largest.

The case studies compare analyses of 1000-500 mb and 700-300 mb thicknesses made from satellite data only with NMC analyses made from conventional data. In addition, isentropic cross sections across baroclinic zones using data from either radiosondes, satellite soundings, or NMC analyses are shown. These cross sections demonstrate that the satellite soundings generally represent the baroclinic zones at least as well as the NMC analyses, with thermal wind speed maxima that are comparable with those obtained from either the radiosonde or NMC analysis cross sections. However, the computed speed maxima from the satellite data were achieved because the soundings depicted the frontal zones as being steeper than in the radiosonde versions. That condition aligned the significant horizontal temperature gradients in a nearly vertical fashion in the satellite cross sections and thus contributed to the vertical summation of the gradients, although temperature gradients at individual levels were usually weaker than the corresponding radiosonde gradients.

1. INTRODUCTION

TIROS N type vertical temperature sounders have been in full operation since early 1979, first on the TIROS N satellite and later in 1979 on the NOAA 6 satellite. A continual question in the minds of operational users and researchers alike is the accuracy and reliability of the sounding data and its capability for depicting the atmospheric thermal structure. A description of the TIROS N Operational Vertical Sounder (TOVS) and evaluations of early operational temperature soundings from TIROS N are found in articles for GARP topics by Smith et al. (1979) and Phillips et al. (1979) in the Bulletin of

the AMS. This report in essence constitutes additional evaluations of later data from the first two satellites in the new series.

As pointed by Phillips et al. (1979), there are some new capabilities in the sounding instruments on board these satellites, and the procedures to use these capabilities are in a more or less continuous state of development and evolution. Evaluation studies themselves constitute a part of the improvement process; certainly no particular evaluation represents the last word on either the accuracy or the capability of the sounding data.

The evaluations in this study are of two types: statistical comparisons between satellite soundings and radiosondes; and case studies of specific synoptic situations to determine how well the soundings describe the atmospheric structure. The standard in either approach is the radiosonde, or analyses derived therefrom. As has been pointed out frequently, the radiosondes themselves include some error, and there is a most significant difference in the size of the volume of air sampled by the two types of instruments. It is the nature and ability of the radiosonde to measure fine vertical structure along a path, and it is the ability of the satellite instruments to measure average atmospheric conditions for a volume. Thus, there is a major difference in the vertical and horizontal resolution of the two instruments.

2. INSTRUMENT SYSTEM AND RETRIEVAL PROCESS

Details of the TOVS instrument system and the processing systems for transforming radiances into profiles of atmospheric temperature are contained in Smith et al. (1979) and Phillips et al. (1979), so only a summary of the essential aspects of these systems, from those two papers, will be presented in this report.

TIROS N and NOAA 6 contain the same instrumentation, and soundings are produced from three instruments: the High Resolution Infrared Radiation Sounder (HIRS), the Microwave Sounding Unit (MSU), and the Stratospheric Sounding Unit (SSU). For temperatures in the portion of the atmosphere of concern in the report, only radiances from the first two instruments are used. These sense atmospheric temperature in the 3.7-μm, 15-μm, and microwave regions, the Earth's surface temperature in three infrared and one microwave region, atmospheric water vapor in three channels, atmospheric ozone in one channel, and reflected solar radiation in one channel. Table 1 provides the characteristics and purpose of the radiance observations provided by the various spectral channels, and the weighting functions for each channel are shown in figure 1. Each curve in the figure displays the vertical resolution of the radiation within a given channel and shows the sensitivity of the radiance to a local variation in atmospheric temperature.

These polar orbiting satellites keep a constant equator crossing time (local); TIROS N and NOAA 6 respectively, pass a point on the equator at approximately 1500 and 1900 local time going northward and at approximately 0300 and 0700 local time southward. They complete about 14 orbits per day with a westward shift of about 25.5° longitude between adjacent orbits. The

TABLE 1. Characteristics of TOV sounding channels.

HIRS Channel number	Channel central wavenumber	Central wavelength (μm)	Principal absorbing constituents	Level of peak energy contribution	Purpose of the radiance observation
1	668	15.00	CO_2	30 mb	*Temperature sounding.* The 15-μm band channels provide better sensitivity to the temperature of relatively cold regions of the atmosphere than can be achieved with the 4.3-μm band channels. Radiances in Channels 5, 6, and 7 are also used to calculate the heights and amounts of cloud within the HIRS field of view.
2	679	14.70	CO_2	60 mb	
3	691	14.50	CO_2	100 mb	
4	704	14.20	CO_2	400 mb	
5	716	14.00	CO_2	600 mb	
6	732	13.70	CO_2/H_2O	800 mb	
7	748	13.40	CO_2/H_2O	900 mb	
8	898	11.10	Window	Surface	*Surface temperature* and cloud detection.
9	1 028	9.70	O_3	25 mb	*Total ozone* concentration.
10	1 217	8.30	H_2O	900 mb	*Water vapor sounding.* Provides water vapor corrections for CO_2 and window channels. The 6.7-μm channel is also used to detect thin cirrus cloud.
11	1 364	7.30	H_2O	700 mb	
12	1 484	6.70	H_2O	500 mb	
13	2 190	4.57	N_2O	1 000 mb	*Temperature sounding.* The 4.3-μm band channels provide better sensitivity to the temperature of relatively warm regions of the atmosphere than can be achieved with the 15-μm band channels. Also, the short-wavelength radiances are less sensitive to clouds than those for the 15-μm region.
14	2 213	4.52	N_2O	950 mb	
15	2 240	4.46	CO_2/N_2O	700 mb	
16	2 276	4.40	CO_2/N_2O	400 mb	
17	2 361	4.24	CO_2	5 mb	
18	2 512	4.00	Window	Surface	*Surface temperature.* Much less sensitive to clouds and H_2O than the 11-μm window. Used with 11-μm channel to detect cloud contamination and derive surface temperature under partly cloudy sky conditions. Simultaneous 3.7- and 4.0-μm data enable reflected solar contribution to be eliminated from observations.
19	2 671	3.70	Window	Surface	
20	14 367	0.70	Window	Cloud	*Cloud detection.* Used during the day with 4.0- and 11-μm window channels to define clear fields of view.

MSU	Frequency (GHz)	Principal absorbing constituents	Level of peak energy contribution	Purpose of the radiance observation
1	50.31	Window	Surface	*Surface emissivity* and *cloud attenuation* determination.
2	53.73	O_2	700 mb	*Temperature sounding.* The microwave channels probe through clouds and can be used to alleviate the influence of clouds on the 4.3- and 15-μm sounding channels.
3	54.96	O_2	300 mb	
4	57.95	O_2	90 mb	

SSU	Wavelength (μm)	Principal absorbing constituents	Level of peak energy contribution	Purpose of the radiance observation
1	15.0	CO_2	15.0 mb	*Temperature sounding.* Using CO_2 gas cells and pressure modulation, the SSU observes thermal emissions from the stratosphere.
2	15.0	CO_2	4.0 mb	
3	15.0	CO_2	1.5 mb	

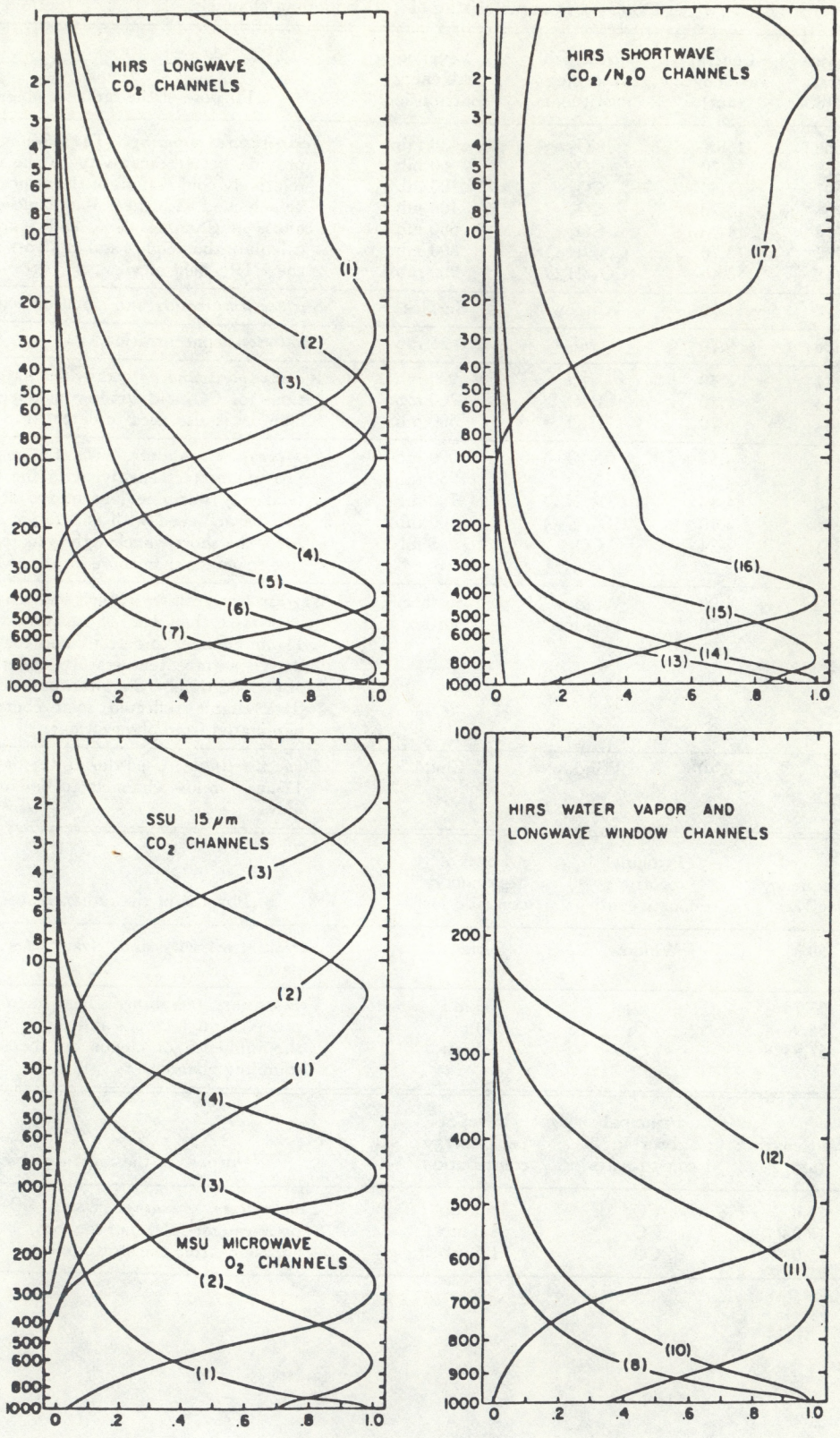

FIG. 1. TOVS weighting functions (normalized).

scan width of the instruments results in overlapping of views poleward of 38°. Each HIRS measurement (scan spot) resolves a circular area that is 30 km diameter at the subsatellite point, whereas the MSU resolves a circular area of 110 km diameter at the satellite subpoint. The fields of view enlarge and become elliptical as the instruments scan away from the satellite subpoint. Fifty-six HIRS spots are contained within each scan line covering a linear distance of about 2250 km. The MSU instrument has 11 fields of view along its swath having the same linear extent. A sounding is made for every array of seven HIRS scan lines and nine spots, resulting in 5 x 6 array of profiles for each 40 x 56 array of scan spots. The nominal horizontal resolution of soundings from TOVS is about 250 km.

The conversion of measured radiances to temperature profiles requires many adjustments to produce the final radiances from which temperatures are produced using linear regression coefficients. These include adjustments for the changing scan angle, surface emissivity, and clouds. Two particularly relevant features of the techniques used to produce temperatures below 100 mb will be discussed briefly.

Temperature profiles are produced from "clear radiances" that have been corrected for any clouds that are inferred to be present. The processing program that produces clear radiances first attempts to identify scan spots that are completely clear. Failing in this, the program then attempts to extract clear radiances from scan spots that are only partly covered with clouds. If this too fails, it attempts to produce temperatures from the four microwave channels and the four stratospheric HIRS channels, since the latter measurements are not as significantly affected by clouds as are the tropospheric HIRS channels. These are in essence the three retrieval methods or paths and will be identified as 1, 2, and 3 for clear, partly cloudy, and cloudy, respectively. Path 1 and 2 retrievals use radiances from all 24 HIRS and MSU channels, and identical coefficients are used to convert from radiance to temperature. However, path 3 retrievals use a different set of coefficients, because a different set of radiances is used.

One would expect path 1 retrievals to be more accurate than path 2 retrievals because of the special assumptions involved in the second method. However, the difference between the path 3 retrievals and either the path 1 or 2 retrievals is greater than the difference between path 1 and 2 retrievals. In addition, the relative accuracies of the three types are sensitive to limits in tests used to accept or reject the attempted retrievals. For example, inclusion of some partly cloudy measurements in the ones selected as clear will decrease the accuracy of this group of soundings. Also, the decision about the retrieval method selected involves tests that are only indirectly related to cloud amounts. These tests involve comparisons between measured and expected albedo and surface temperatures, and between a measured microwave radiance and a microwave radiance predicted from those infrared radiances that are subject to cloud contamination. Radiances from the 15-μm region are also used to predict radiances of the 4.3-μm channels, which are compared to measured values.

The second important feature of the processing procedure is the regression for atmopsheric temperature alluded to above. Regression coefficients for a given latitude zone are updated weekly using collocated radiosonde and satellite data uniformly distributed over the preceding two weeks. Coefficients are then used for the following week. This procedure results in an average time lag ranging from one and one-half weeks in a data-rich region to two and one-half weeks in a data-sparse region (it takes longer to collect a given quantity of collocations). Separate regression coefficients are calculated for each of five latitude zones: two zones from 60° latitude to the poles, two zones from 30° and 60° latitude, and one tropical zone from 30°N to 30°S.

To eliminate temperature discontinuities that would otherwise occur at 30° and 60°, the coefficients used for a retrieval are interpolated from those for the five zones. In the interpolation, the highest-peaking microwave channel (57.95 GHz), which senses the upper troposphere and lower stratosphere, is used to interpolate between latitude zones. When coefficients are generated, the average value of the brightness temperature for this channel is calculated for each zone. If the three average values for a hemisphere are monotonic (the usual condition in summer), then the value of this channel for a particular sounding is used to determine the two latitude zones whose values bracket the observation, and the resulting profile is the weighted average between the results obtained with the two latitude zones. If the sounding is not bracketed because it falls outside the range of the three average values, no weighting is performed, and coefficients from the nearest latitude zone are used. Also, no weighting is allowed between 15°N and 15°S. If the three average values for a hemisphere are not monotonic (the usual condition in winter), then it is not possible to decide which zones to use. In this situation, all soundings poleward of 45° are weighted between polar coefficients and midlatitude coefficients. Similarly, equatorward of 45° weighting is performed between midlatitude and tropical coefficients.

The instrumentation and the processing of the radiances from the sounders on the two satellites were essentially the same, with the notable exception that the MSU channel 3 on NOAA 6 was not used from early December 1979 until after the end of the period in this study, because it was considered too noisy.

3. STATISTICAL EVALUATION

The statistical portion of this evaluation is derived from a data set produced operationally. These sets are comprised of collocated and radiosonde observations. Collocation means that some standard of acceptable separation or "window" must be set. The spatial "windows" are smallest in regions of high density radiosonde coverage and vary from 1° lat./long. in the Northern Hemisphere middle latitudes to 2° in the polar and tropical regions. A 3° "window" is used everywhere south of 10°N. There is no time window per se, since the radiosonde data are interpolated to the time of the satellite observations from two bracketing radiosonde observation times. These collocated data have been collected for the five broad latitude zones corresponding to the latitude zones used for calculating retrieval coefficients (60-90N/S, 30-60N/S and 30N-30S). The statistical comparisons have been summarized by satellite (TIROS N or NOAA 6), month, retrieval path

(1, 2,or 3), and terrain (land or water). We will show the results of these comparisons for the 30N - 60N latitude zone because radiosonde coverage is best in this latitude belt, the zone covers the active extratropical westerlies, and the volume of results is reduced.

All comparisons are for mean layer temperatures defined by the mandatory pressure levels. The radiosonde geopotential height at each level was used to determine the thickness for each layer and, assuming dry air, these were converted to layer mean temperatures using the hydrostatic equation. Similarly, the layer mean temperatures were calculated for the satellite retrievals. Comparisons are confined to the nine layers defined by the mandatory pressure levels up to 100 mb.

The statistical parameters shown are for a period from September 1979 through April 1980, a time when both satellites were producing soundings operationally. The error statistics calculated are the root mean square (RMS) and the mean temperature differences between the satellite and the radiosonde matches. These statistical parameters are shown separately in graphical form and stratified by satellite, terrain type, retrieval path, and month, in that order of breakdown. The graphs are isoplethed and shaded to make it easier to grasp the picture they present. Four pairs of figure graphs (both satellites for each of the four combinations of RMS or mean difference and land or sea) are shown in figures 2-5 (a and b). The RMS values represent the total spread of the measured data about the verifying data and will be discussed first.

One all-pervasive effect can be seen in the four figures showing the RMS values for the two satellites over both land and sea (figs. 2a, 2b, 3a, and 3b). The RMS values are largest in the layers closest to the surface of the Earth and in the layers containing the upper troposphere and tropopause region. Minimum RMS values are therefore associated with the mid-troposphere and the low stratospheric layer at the top of the diagrams. The two maxima are a consequence of temperature structure combined with the low vertical resolution of the sounder. Broad weighting functions simply cannot capture the stable layers, inversions, and other highly variable temperature structures found near the surface and tropopause. Since the mid-troposphere, except in baroclinic zones, is generally more simply structured both in the vertical and horizontal, sounding retrievals here do rather well on the whole.

Looking at the individual vertical regions mentioned above with respect to the cloud-dependent retrieval types, one can see that the lower-layer maximum definitely increases in magnitude and extent going from clear to cloudy conditions. Also, the mid-tropospheric minimum definitely decreases in extent from clear to cloudy conditions. Looking at the tropopause maximum, one can see that it tends to increase in extent from clear to cloudy regions, most obviously for TIROS N land and NOAA 6 sea conditions (figs. 2a and 3b). The highest layer minimum shows a tendency to increase in extent, i.e. improve, when proceeding from clear to cloudy conditions. This improvement is probably reasonable, since one should be able to retrieve this high layer in the presence of clouds, and at the same time there may be less variability in this layer for any given sample.

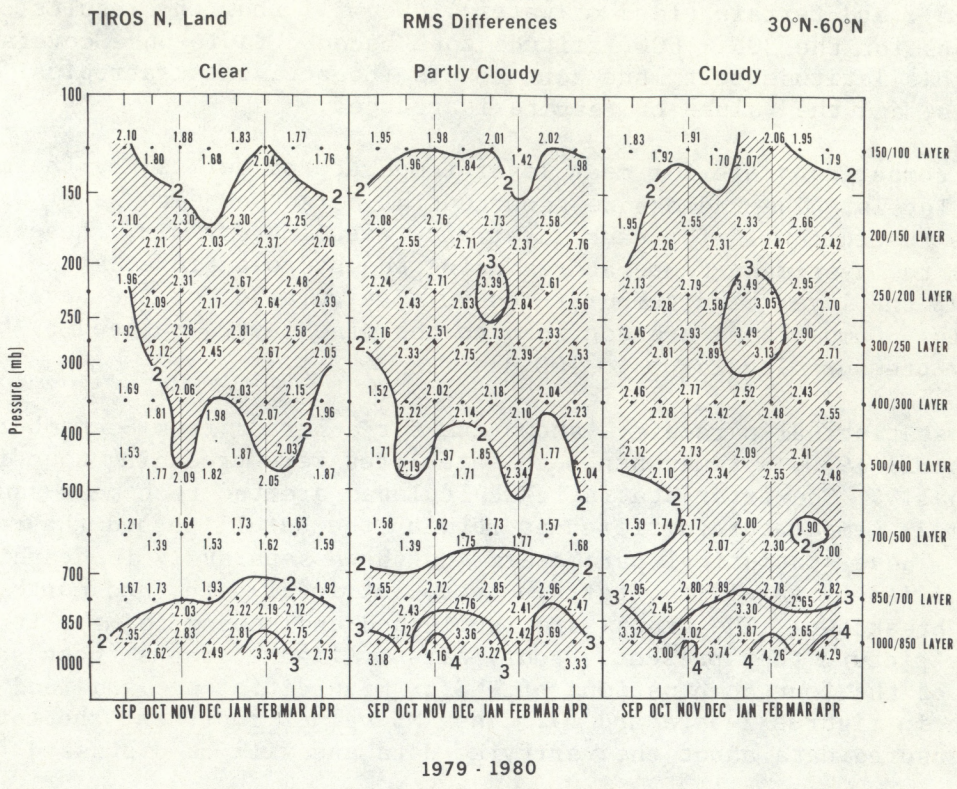

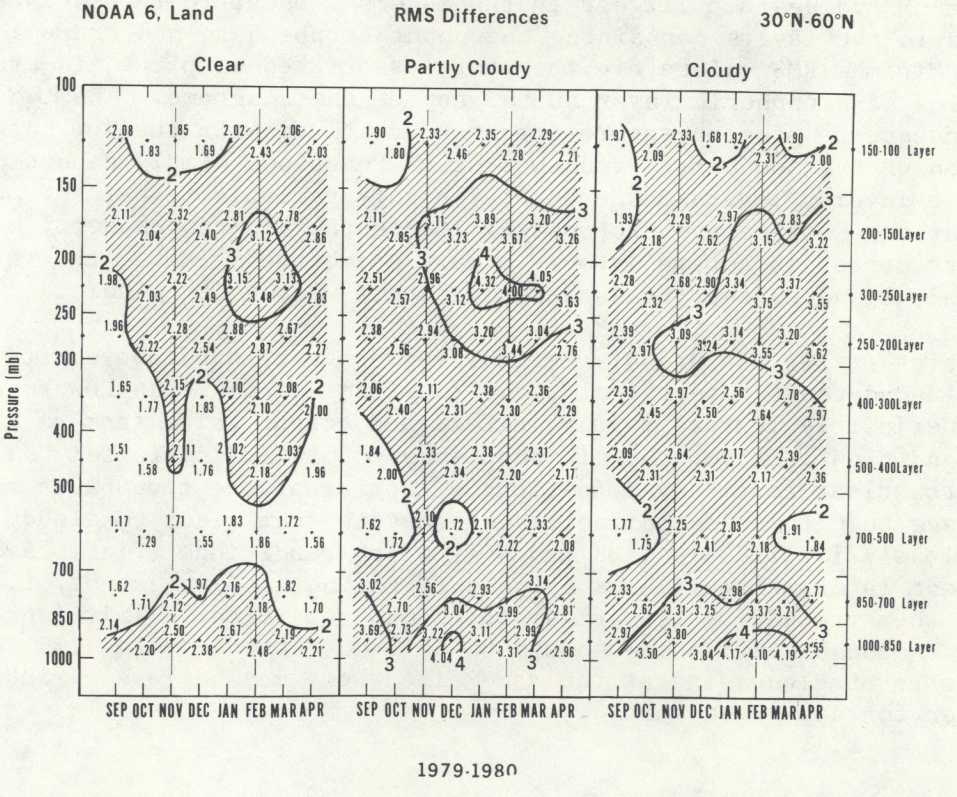

Figure 2.--RMS differences between satellite retrieval and radiosonde layer mean temperatures for 30° - 60°N. Hatching indicates RMS values greater than 2°. a) TIROS N over land, b) NOAA 6 over land.

The next aspect of the RMS diagrams we will examine is the seasonal or time variations within the several sections of atmosphere previously discussed. In the boundary layers generally the seasonal variation appears to be indistinct, with only a slight tendency for the RMS values to be larger in the winter months. In the mid-tropospheric layers under both clear and cloudy conditions, both satellites over land and sea do show some increase in RMS going into winter and a slight decrease in spring. This tendency is most noticeable for the clear TIROS N sea retrievals (fig. 3a). For the tropopause region of the atmosphere, both satellites over land and sea under all retrieval conditions show an increase or a tendency for an increase in RMS values going into the winter months but with varying tendencies to decrease into the spring months.

Altogether, then, the RMS values in these figures for this relatively short period, that doesn't include summer months, show a relatively mild and non-uniform seasonal relationship. However, there is some overall tendency for the increase in RMS values into winter and some slight decreases in the early spring months that one generally expects because of the greater atmospheric variability during the colder part of the year.

Another aspect of the comparisons of interest is that of land versus sea retrievals. For TIROS N under clear conditions the sea RMS values are somewhat larger in the mid-tropospheric and tropopause layers, and for partly cloudy the sea retrievals have distinctly larger RMS values in the middle and tropopause layers. The RMS values for cloudy conditions in the middle layers tend to be slightly smaller for the land values and in the tropopause layers slightly larger than the sea values.

For NOAA 6 the land-sea differences are even less well-defined than those for TIROS N. Under clear conditions the RMS values for the sea tend to be somewhat larger in the tropopause layers. The land values for the low layers under partly cloudy retrievals tend to be somewhat larger. For cloudy conditions it is difficult to find any noticeable or consistent differences between land and sea throughout all of the layers considered here.

In general, then, for TIROS N the land RMS values would tend to be better (smaller) than the sea RMS values for clear and partly cloudy conditions with little difference for cloudy conditions, whereas for NOAA 6 the land and sea values tend to be more nearly comparable throughout the three types of cloud conditions.

Next, we discuss the mean or bias differences in the comparisons, shown in figures 4a, 4b, 5a, and 5b. First to be discussed are the means for TIROS N and NOAA 6 over land. Before going to the various atmospheric sections, some general statements will be made. Some tendency can be observed for the mean differences to be larger in the lowest layers and in the tropopause layers, although this does not stand out as clearly or consistently as in the case with the RMS values. The biases are generally positive in the tropopause region for TIROS N, with the largest being for cloudy conditions, whereas the biases are not consistently positive for NOAA 6 except for partly cloudy conditions.

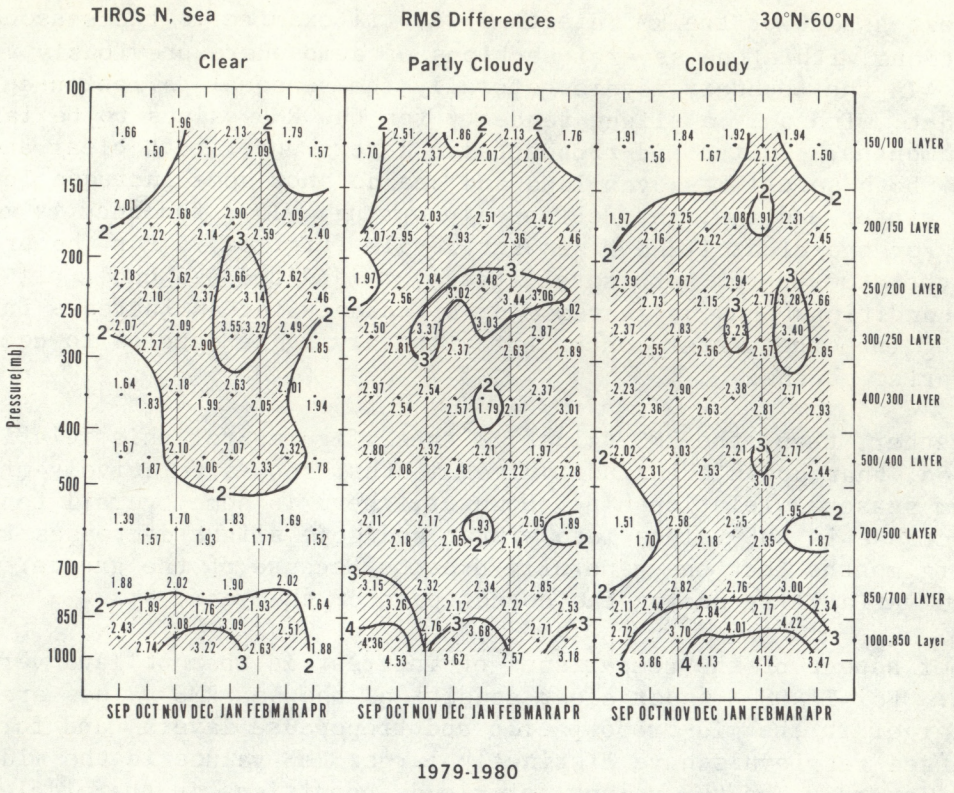

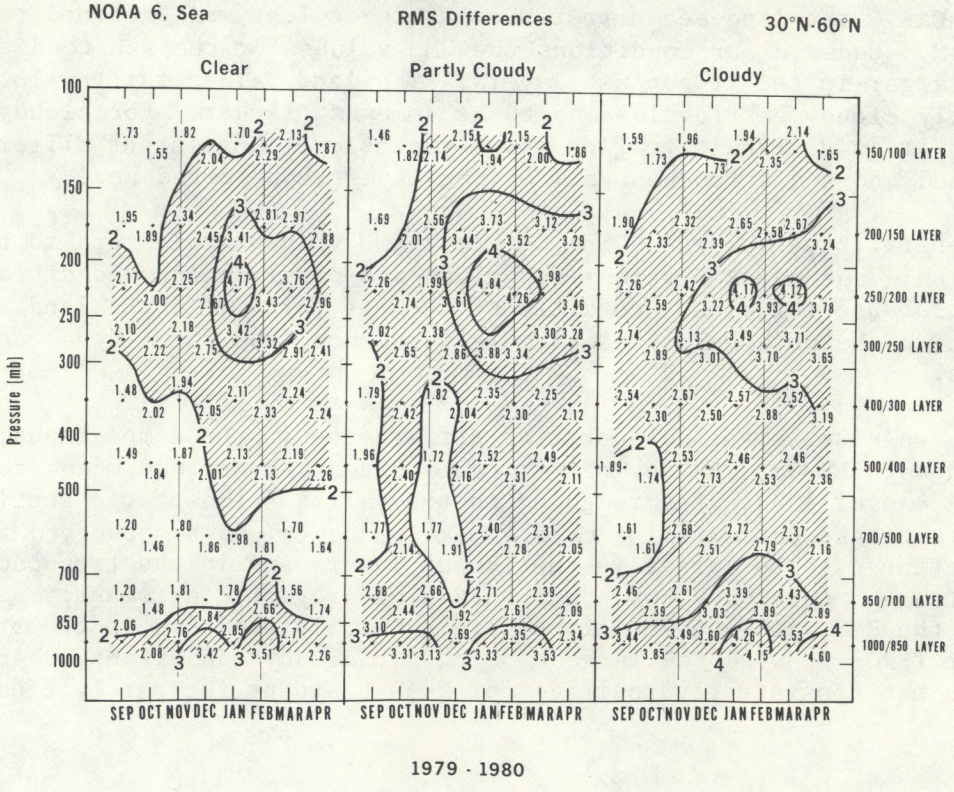

Figure 3.--Same as figure 2. a) TIROS N over sea; b) NOAA 6 over sea.

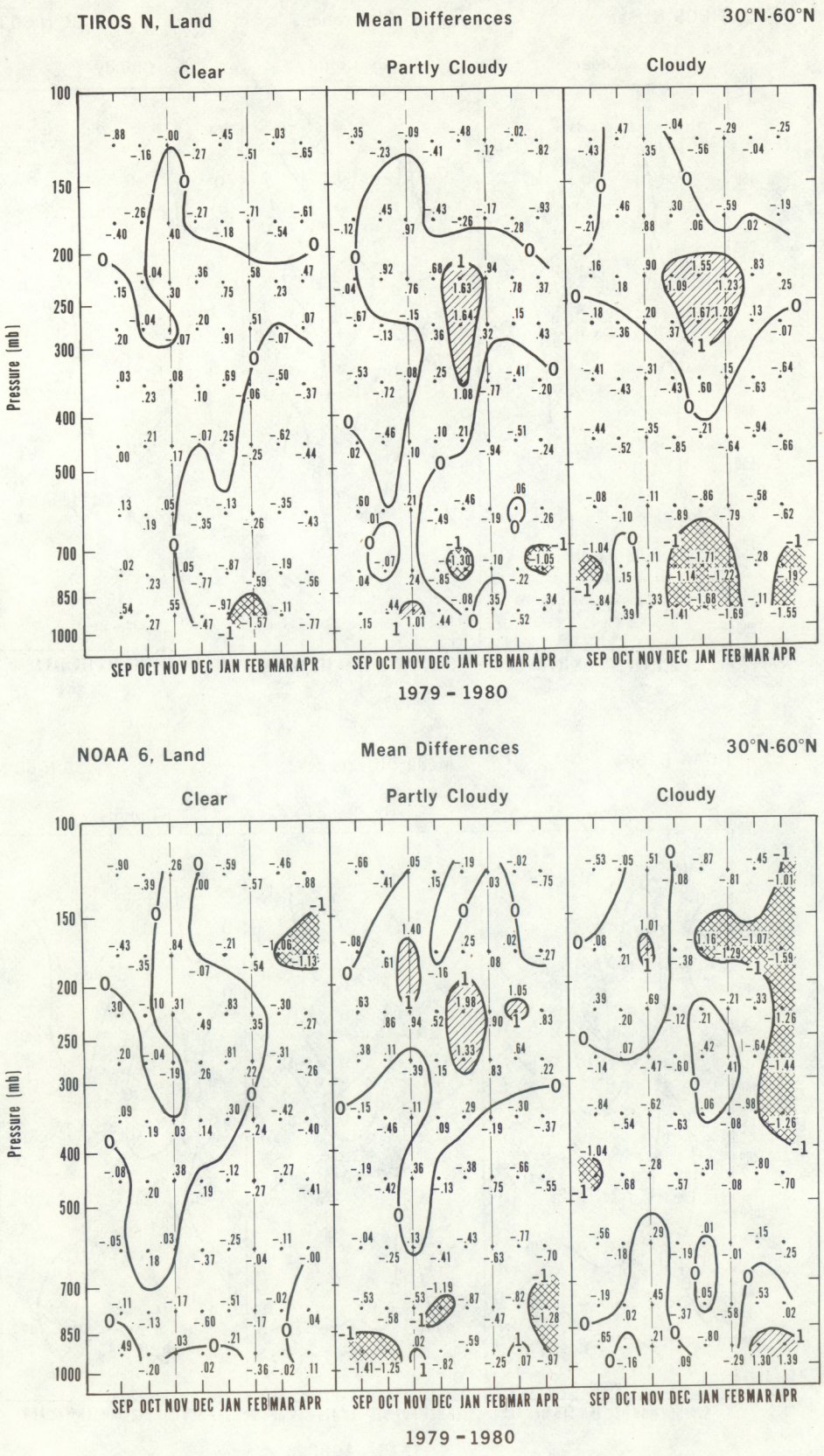

Figure 4.--Mean differences between satellite retrieval and radiosonde layer mean temperatures for 30° - 60°N. Hatching indicates mean difference values greater than 1° (+ or -). a) TIROS N over land, b) NOAA 6 over land.

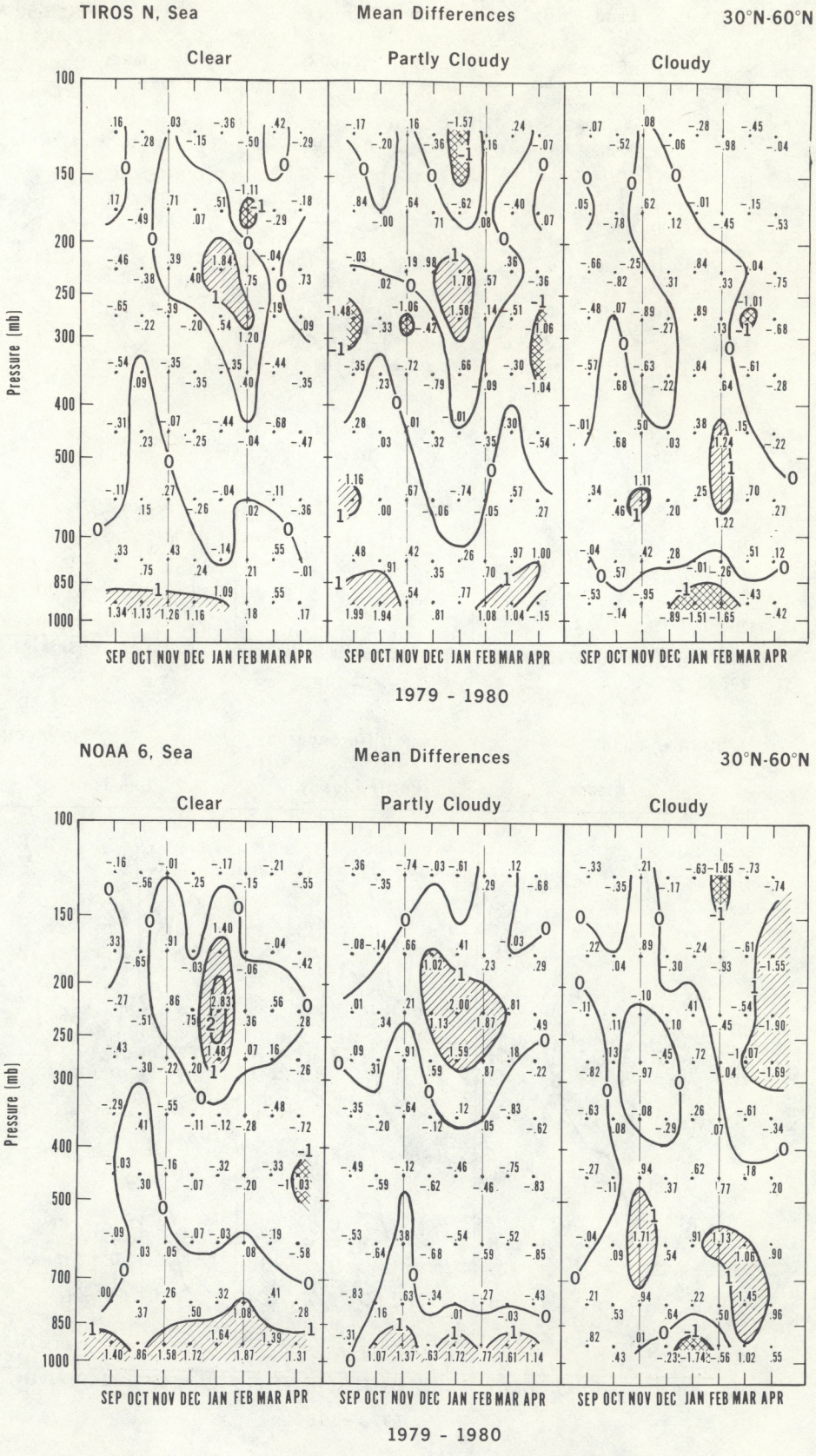

Figure 5.--a) TIROS N over sea; b) NOAA 6 over sea.

Looking now at individual sections of the atmosphere, we see that in the lowest layers for clear conditions both satellites have rather small biases in fall and spring with larger cold biases in the winter period; however, TIROS N definitely has the larger values. The biases for cloudy retrievals are rather consistently larger than those for clear retrievals. Non-uniform variations between the satellites can be noticed such as NOAA 6 having larger values than TIROS N for partly cloudy conditions, but as in the clear sky conditions, TIROS N cloudy retrievals tend to have larger mean differences than NOAA 6. Also, the TIROS N cloudy cases have a markedly cold bias in winter and weaker cold bias in spring, as opposed to a rather weak cold bias for NOAA 6 in winter and a warm bias in spring.

In the mid-tropospheric layers for clear retrievals the biases are small for both satellites during fall and winter with a tendency for a slight increase and a cold bias in the spring. Also, for both satellites the bias tends to increase in size from clear to cloudy conditions. For all cloud conditions, and both satellites, the biases are largest in the spring period.

Considering the tropopause region, one finds that for both satellites clear conditions produce the smallest biases. Both satellites show a warm bias for partly cloudy conditions during the winter, which weakens and carries into the spring. TIROS N cloudy retrievals also show a warm bias during the winter, but NOAA 6 tends to have a cold bias. The TIROS N warm bias weakens considerably and carries into spring, whereas the NOAA 6 cold bias strengthens markedly as it carries into spring.

There is an interesting relationship between the biases just described for the two satellites under cloudy conditions during winter and spring. As pointed out earlier for the low layers, NOAA 6 is warmer than TIROS N, and for the tropopause layers just discussed NOAA 6 is colder than TIROS N by significant amounts. This combination of bias differences between the two satellites coincides with the elimination of MSU channel 3 in the NOAA 6 instrument from the retrieval process early in December 1979 because it was thought to be too noisy for use. This channel peaks near 250 mb so that an effect in the tropopause layers is understandable, but these results suggest a possible effect in the low layers as well.

Pursuing the preceding relationship further, it can be noted from the RMS diagrams that, while the RMS values of the two satellites under cloudy conditions are quite comparable for the fall period, there is a definite increase in the NOAA 6 values in the tropopause layers during the winter and spring months. A simulation study of a dependent data set by Grody (1980), with and without MSU channel 3, showed that there was up to 1.5°K increase in the RMS error near where the weighting function peaks, around 250 mb, when channel 3 was not used. In addition, the study showed there was about .5°K error increase below 850 mb, which suggests there is generally a statistical connection between the upper and lower levels, and agreeing with results noted in the preceding paragraph. The increase of NOAA 6 RMS values in the tropopause region during winter was pointed out in Gruber et al. (1980), where it was also noted that an increase showed up in the NOAA 6 clear RMS values for winter. The increase of RMS in clear cases can be seen in these RMS

diagrams for spring as well, and in addition, it is seen in the partly cloudy conditions. The similar effect of the lack use of MSU channel 3 in path 1 and 2 retrievals apparently reflects the importance of this channel in the tropopause region even when all of the infrared channels are being used. It can be seen in figure 1 that MSU channel 3 fills in a gap left by the HIRS channels.

Turning to the mean differences over the sea and starting with the lowest layers, both satellites under clear and partly cloudy conditions tend to have a consistently warm bias through all seasons. For cloudy conditions TIROS N has a small cold bias in fall and spring and a moderate cold bias in winter, whereas NOAA 6 tends to have a rather small warm bias in fall, a modest warm bias in spring, and a modest cold bias in winter. NOAA 6 thus has a bias that is warmer relative to TIROS N for cloudy conditions.

For the mid-tropospheric layers, the clear retrievals show a cold bias for both satellites in the spring that increases to fairly moderate magnitudes. Under partly cloudy conditions NOAA 6 has a relatively small cold bias in fall and winter that increases to a moderate size in the spring. Both satellites under cloudy conditions have rather moderate warm biases in the winter.

In the layers around the tropopause region, both satellites show warm bias for clear and partly cloudy conditions during winter, especially NOAA 6. Both satellites during spring cloudy conditions have cold biases, which become rather large for NOAA 6.

As over the land, NOAA 6 has a relatively warmer bias in the low layers in winter and spring for cloudy conditions and a relatively cold bias in the tropopause layers. However, the situation over the sea is not nearly as pronounced as it is over the land.

3.1 Summary

The most obvious feature seen in the statistics, regardless of the satellite, retrieval path, or underlying surface, is that the RMS values are largest in the layers closest to the surface and in the layers containing the tropopause region. Minimum RMS values are found in mid-tropospheric layers.

In regard to retrieval path, the clear retrievals are definitely the best in all seasons and in all layers but the very highest one, with the cloudy retrievals having consistently larger RMS values. The general tendency is for the partly cloudy retrievals to have RMS values somewhere between clear and cloudy.

The length of this sample is rather short to evaluate seasonal trends; however, in the mid-tropospheric and tropopause regions there is a tendency for an increase of RMS values from fall into winter under most conditions, but with much weaker and sporadic indications of any decrease following the winter months. These slight decreases may not be surprising, since the sample goes

only into early spring when there is still considerable atmospheric variability likely to be present.

A comparison of the RMS values between satellites was only partially covered in the discussion, but it appears from the diagrams shown that the two satellites are about comparable, or nearly so, under most conditions in most regions of the atmosphere, except in the tropopause layers where the lack of use of microwave channel 3 on NOAA 6 gave a distinct advantage to the quality of the TIROS N retrievals.

In general, differences in RMS values between land and sea are not well defined, but TIROS N tends to show more difference between the two than NOAA 6. For TIROS N the RMS values for sea retrievals tend to be larger in the middle layers and also for the tropopause layers under clear and partly cloudy conditions. Land and sea RMS values for NOAA 6 are quite comparable or the differences between them are mixed with no distinct edge for either one.

Although there is some tendency for mean differences to be larger in the surface and tropopause layers than in the middle layers, the pattern is not nearly as consistent or well-defined as was the case with RMS values. For TIROS N over land the tropopause region biases are generally positive, but over the sea the sign of the bias is mixed, being consistently positive only in the winter months. In the low layers, the biases for TIROS N over land tend to be negative, but over the sea they are consistently negative only for cloudy conditions. For NOAA 6 the lack of use of the microwave channel 3 from December onward may account for the lack of consistency between the two satellites.

4. CASE STUDIES

Statistical type evaluations, such as presented in the previous section, are useful for determining the general accuracy of the satellite measurements. Such information is necessary for several purposes, e.g. quality control, validation of improvements in retrieval processing, and determining error levels for optimum interpolation analysis procedures. However, statistical evaluations tell little about the precise manner in which the satellite measurements will describe the temperature structure of a particular cyclone system or frontal zone in any given synoptic situation. The purpose of the case studies presented here is to show the thermal patterns in the vicinity of baroclinic zones and examine the manner in which these zones are depicted by the satellite data. Evidence of some of the primary statistical features of the previous section, such as larger RMS errors in the near-surface layers and the tropopause region, will also be seen in the individual cases, but other features of the thermal structure depicted by the satellite data could not be anticipated from the results of the statistical evaluation.

4.1 Data Processing and Analysis

Before discussing the case studies, some of the necessary processing details should be noted. First, a NMC routine was used to convert the layer

mean temperatures provided by NESS to constant pressure level temperatures and thicknesses from 1000 mb to each mandatory constant pressure level. Thus, the satellite soundings used in the study were structured the same as those NMC would use in their operations.

Next, the satellite data were analyzed by a Cressman-type objective analysis scheme. A zero guess field was used on the first scan, and each piece of data was weighted to all grid points within a 5 grid-length radius about its location. A gross error check was then performed between each data value and the interpolated first scan value at its location. If the difference between the two values exceeded a prespecified limit that piece of data was thrown out for the remainder of the analysis. Subsequently, four additional scans were carried out with a successively decreasing radius of influence. A five-point smoother was used after each scan.

Comparisons were made between NMC analyzed fields (which contained no satellite soundings in the April 1979 case and none over land in subsequent cases) and the satellite-only analyses as described above, both by visual inspection and by taking grid-point differences. This was done for analyses at 3 constant-pressure levels, 850, 500, and 250 mbs, and for two thickness layers, 1000-500 mb and 700-300 mb. The 700-300 mb layer was chosen because it is above the lower boundary layer where there are difficulties with the satellite soundings and in the middle troposphere where the retrievals should do well. The NMC analyses used were from the final cycle, which uses the optimum interpolation technique.

Isentropic cross-sections, using a modified form of the Shapiro-Hastings program (1973), were computed individually from satellite retrievals, radiosonde observations, and the NMC temperature analyses. These cross sections include vertically integrated thermal wind speeds computed normal to the orientation of the section. Thermal wind speeds, of course, provide an excellent measure of the horizontal (isobaric) temperature gradients present in the several representations of the atmosphere.

4.2 Case Study - April 6, 1979, 1200 GMT

4.2.1 Synoptic Situation

The surface pressure analysis for 1200 GMT April 6 shows a cold front moving through the east coast States and trailing westward through Arkansas to the Texas panhandle, bringing with it an arctic air mass. An earlier polar air mass covers the region ahead of the cold front. Aloft the cold outbreak is associated with a difluent shortwave trough that had dropped southeastward from Canada into the longwave trough position in the eastern portion of the United States. The strongest temperature gradients and a rather sharply defined speed maximum of the jet stream are located on the southern and western sides of the trough. It is through this portion of the system that the cross sections are taken.

4.2.2 Satellite Data and Analyses

The locations and times of the TIROS N retrievals are shown in figure 6. The area through the midwest where the cross sections are taken is about two hours prior to the time of the radiosondes and NMC analyses. The symbols indicate the type of retrieval path used; open circles for clear, solid circles for cloudy, and stars for the N-star or partly cloudy paths.

The IR cloud picture from TIROS N in figure 7 indicates the primary cloudiness with the shortwave trough is to the northeast of the Great Lakes, with only a weak cloud band oriented NW-SE across the midwest. The cloudy path retrievals from Minnesota northward toward Hudson's Bay (fig. 6) are in a region that is mostly clear according to the surface chart, otherwise the cloudiness in figure 7 seems to be in good agreement with the plotted retrieval paths in figure 6. This discrepancy between the cloudy path retrievals for an apparently clear region may arise because the surface was at such a cold and uniform temperature, as can be seen in the IR picture (fig. 7), that the processing routines (which utilize the window channels) defined the area as cloudy.

The TIROS N and NMC 1000-500 mb thickness analyses are shown in figure 8. The general resemblance of the patterns is quite strong. Over most of the North American region they agree to within ±40 m (2° mean temperature). The cold region in the TIROS N analysis over the mountainous western United States is probably an elevation effect caused by a low temperature from the lowest reported TIROS N layer (still some distance above ground) being reduced to a 1000 mb temperature that is too low, thereby causing the thickness to be too shallow. Note the positive difference region in southern Canada extending southeastward into the central United States and located in the most baroclinic zone. This difference reaches a magnitude of greater than 80 m, and its significance will be explored later. The system with the large negative differences in the Pacific will also be discussed separately.

Examining the 700-300 mb thickness anlayses in figure 9, one can see the agreement between the TIROS N and NMC patterns is excellent over most of the map. The principal exceptions are again large and strong negative differences in the Gulf of Alaska and the negative differences in the northern Great Plains. This latter area corresponds closely to the large difference area of opposite sign previously noted in the 1000-500 mb thickness analyses. Certainly closer scrutiny is warranted to determine the nature of the thermal structure in that region.

The three-dimensional thermal structure of the short wave trough can be assessed with the help of isentropic cross-sections. Three sections and their locations are shown in figure 10 - TIROS N retrievals only, radiosonde only, and NMC analysis extracted at TIROS N locations. Surface and reported tropopause significant levels were added to the radiosonde reports; otherwise only mandatory level temperatures were used in all three types of data. Two features can be noted in comparing these three sections. One is the treatment in the tropopause region where the addition of the tropopause level to the radiosonde profile undoubtedly increases the definition in this cross

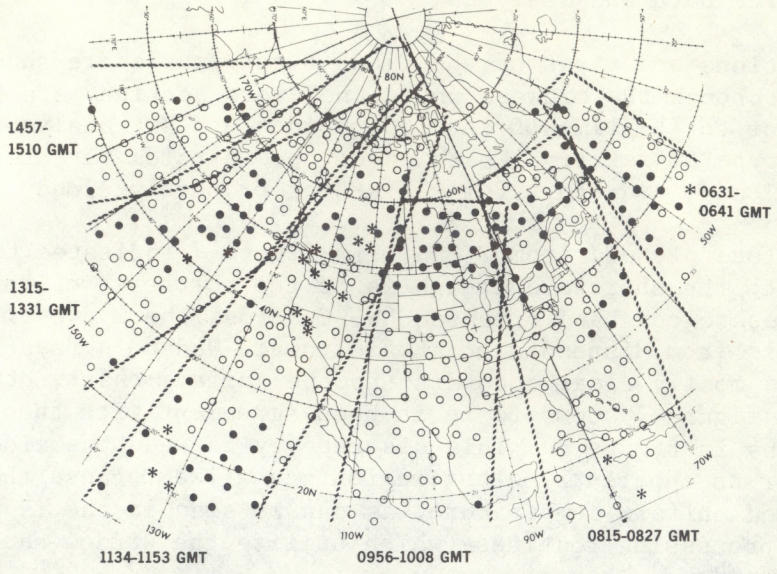

Figure 6.--TIROS N retrieval locations for April 6, 1979. Broken lines delineate orbital swaths with times as indicated. Open circles indicate clear path, stars indicate partly cloudy path, and solid circles indicate cloudy path retrievals.

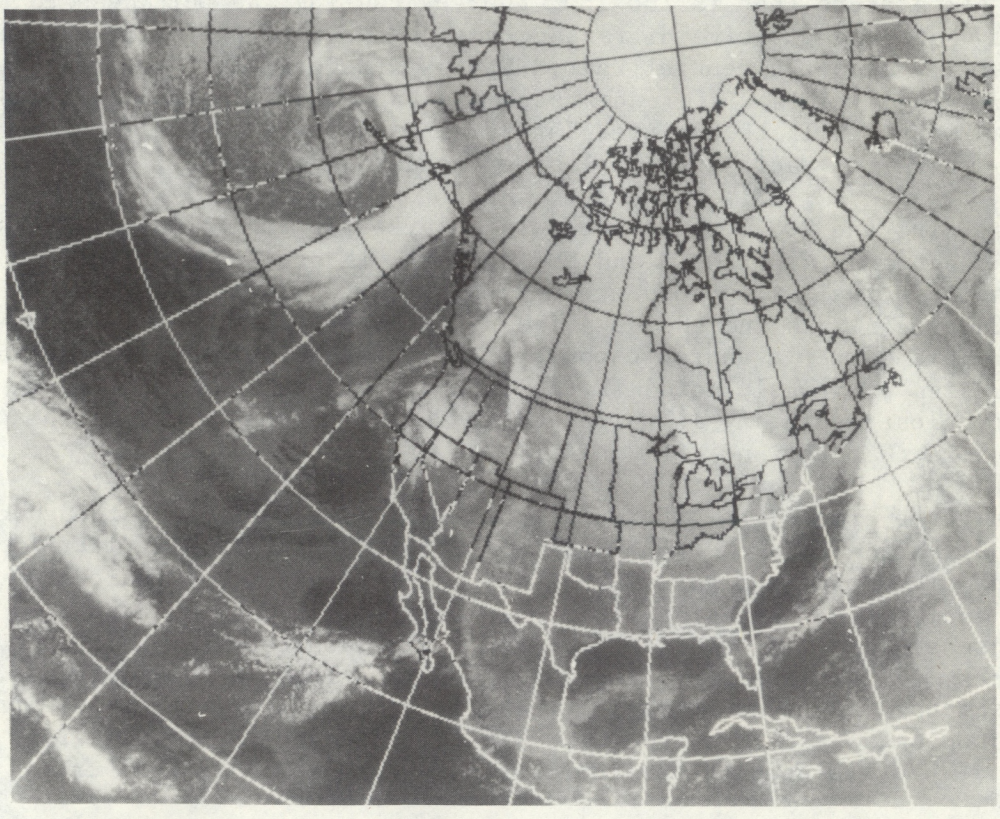

Figure 7.--TIROS N digitized infrared mosaic for April 6, 1979. Time corresponds to swaths in Figure 6.

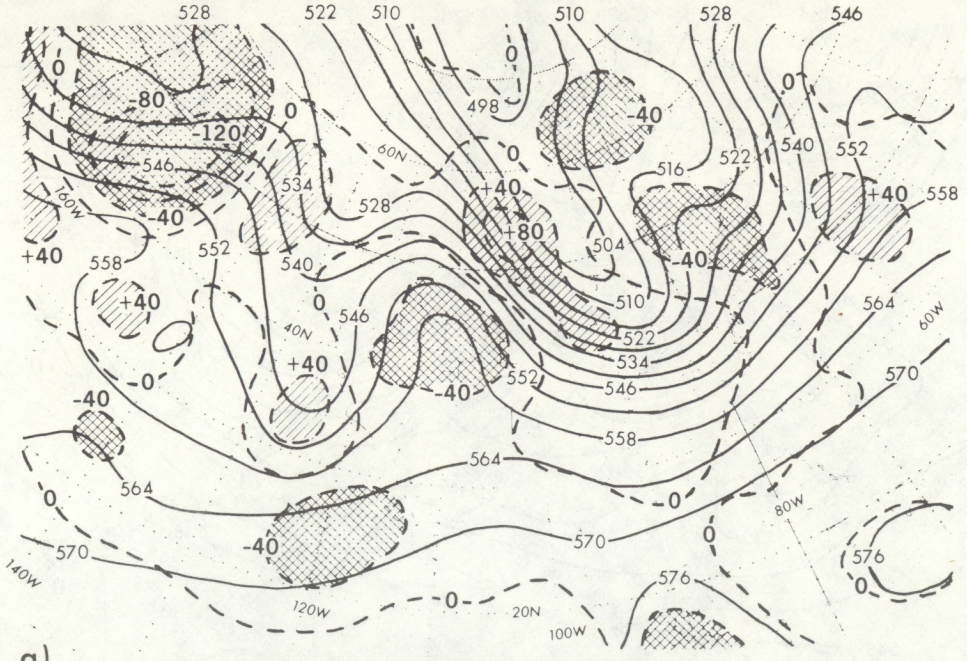

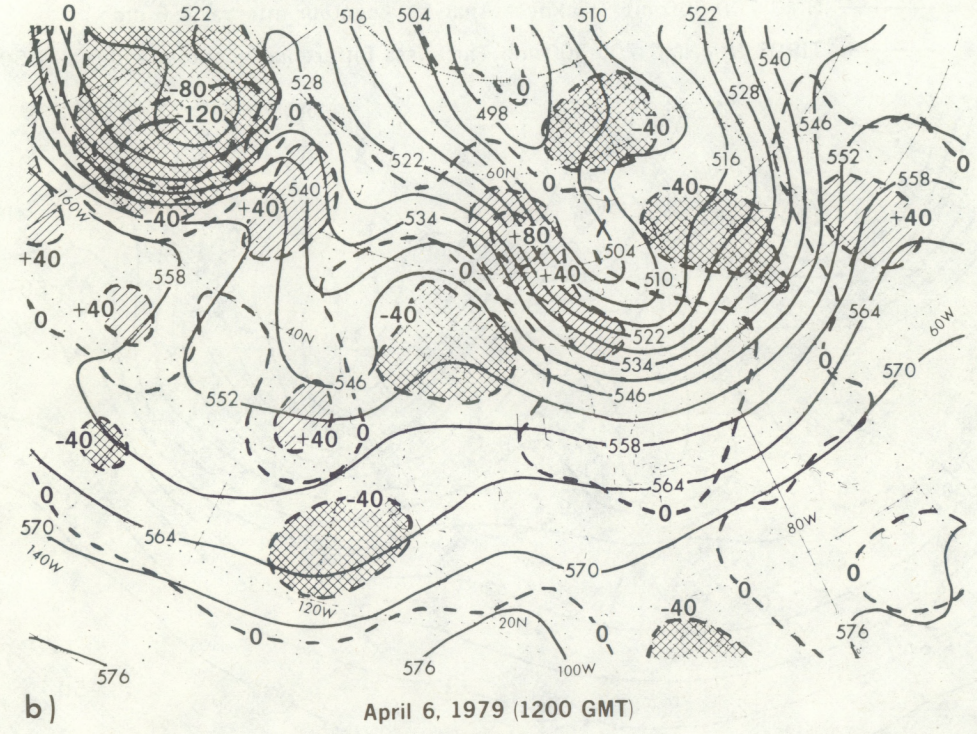

Figure 8.--a) NMC 1000 - 500 mb thickness analysis in solid lines (contour interval = 6 dm), and the broken lines are the TIROS N minus NMC thickness difference (contour interval = 40 m) for 1200 GMT, April 6, 1979. b) TIROS N 1000 - 500 mb thickness analysis in solid lines (contour interval = 6 dm) with broken lines same as a) for about 1000 GMT April 6, 1979.

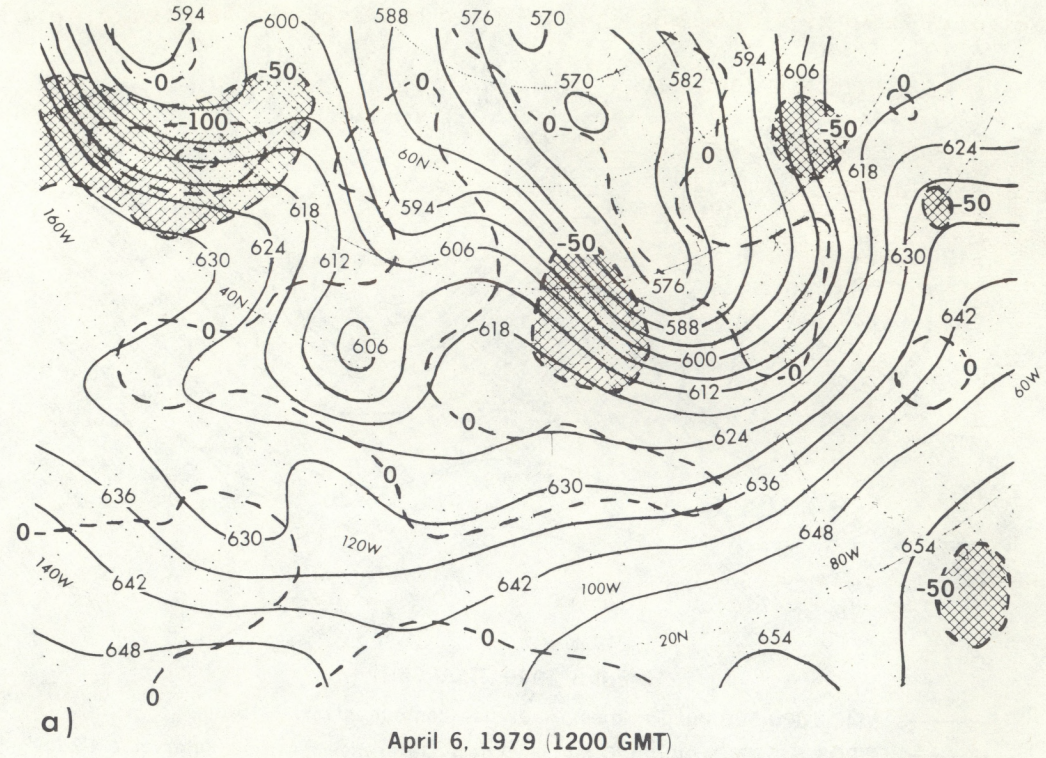

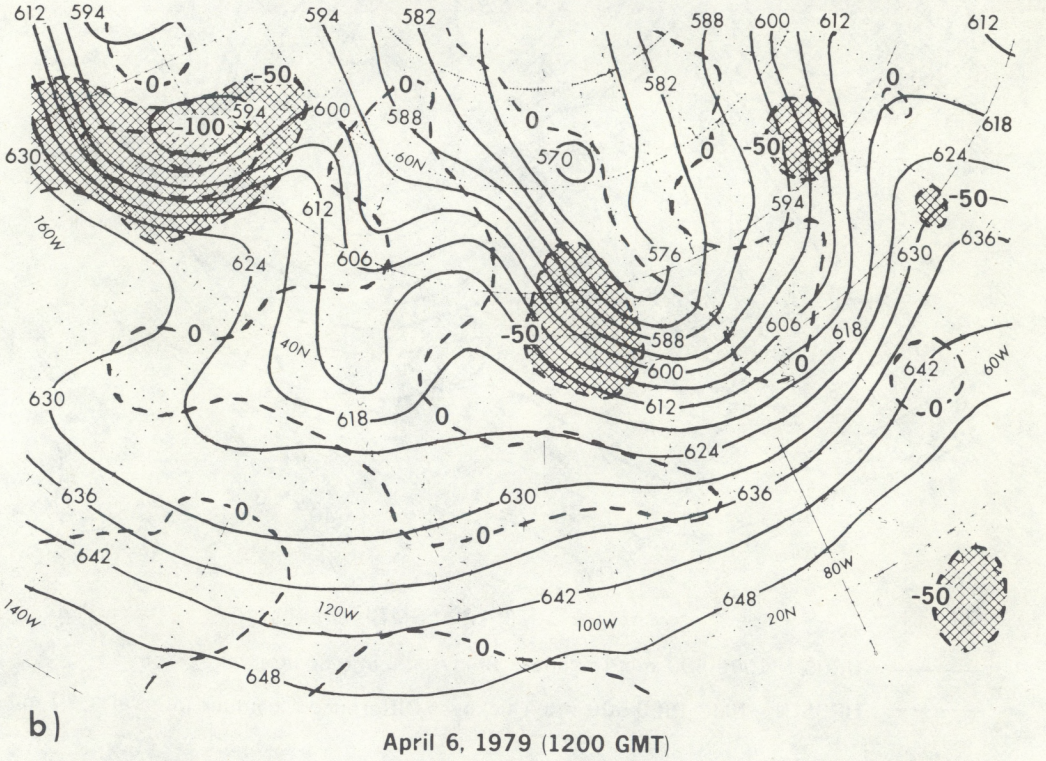

Figure 9.--a) Same as figures 9a) and b) except for the 700 - 300 mb thickness, and the thickness difference contour interval = 50 m.

Potential Temperature (K) and Thermal Wind (m/sec) Cross Sections, 6 April 1979:

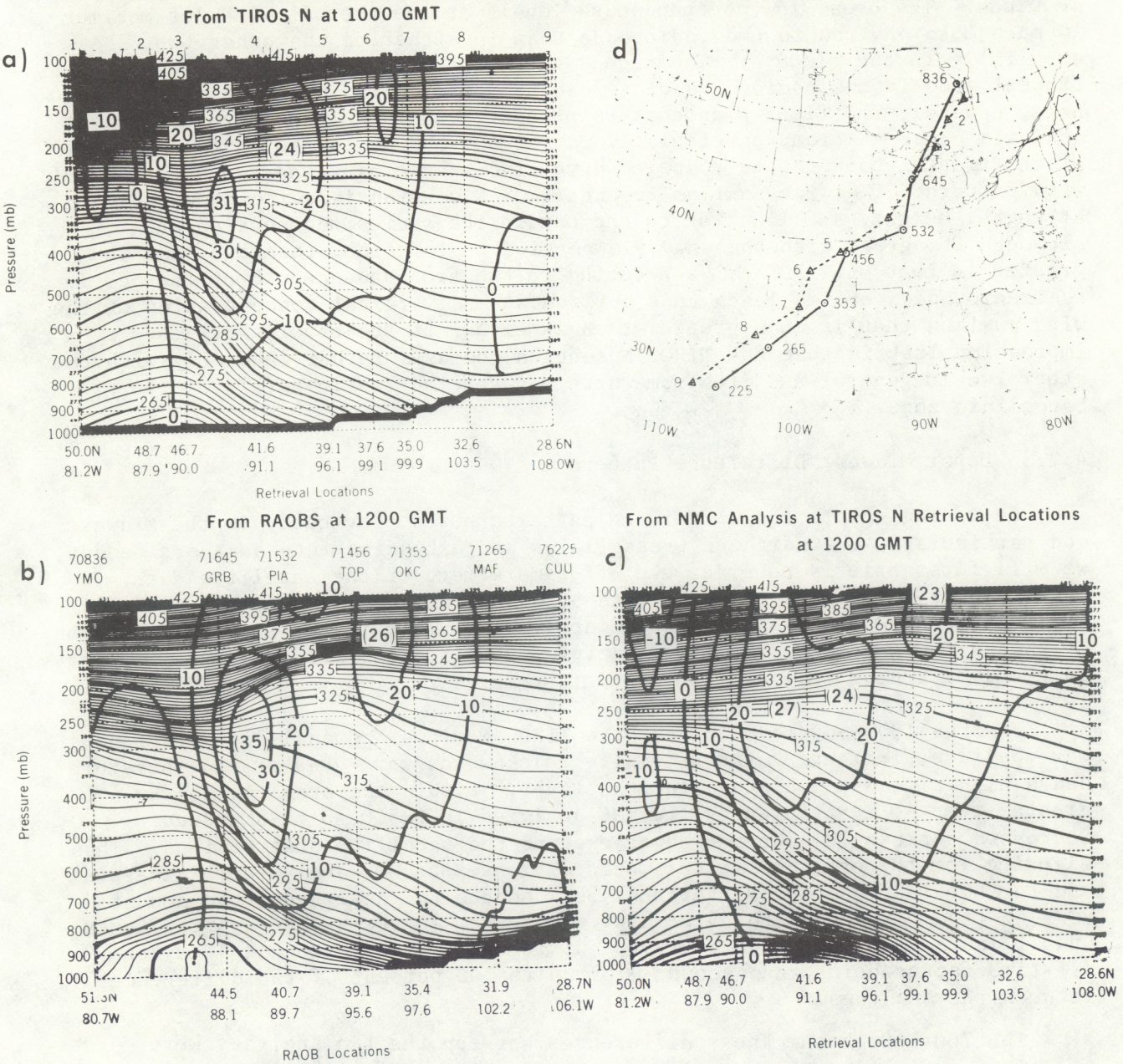

Figure 10.--Isentropic cross-sections for 1200 GMT April 6, 1979 (TIROS N about 1000 GMT). Potential temperature (deg. K) in narrow solid lines and thermal winds in wide solid lines (m/sec). a) TIROS N retrievals, b) radiosondes, c) NMC final cycle analysis at TIROS N locations, and d) TIROS N locations indicated with triangles and broken line, radiosonde locations with circles and solid line.

section. In general, the change in the lapse rate at the tropopause is more apparent in the radiosonde cross-section than in the TIROS N or analysis cross sections. The break in the tropopause levels at the thermal wind jet maximum is much more obvious in the radiosonde than in either of the other two, especially in the TIROS N. The second feature to note is the sharpness of the frontal zone in the radiosonde cross-section as compared with the other two; here, however, the TIROS N appears to present a sharper frontal zone than the analysis cross-section, particularly in the 600-800 mb layer. This strength of the frontal zone can be compared directly by examining the computed thermal wind pattern. The wind maximum in the TIROS N section is quite comparable in strength, height, and location to the one in the radiosonde section and, although it agrees with the analysis section in location, the magnitude is greater in that of TIROS N. The doming in the tropopause south of the jet in the radiosonde section leads to a horizontal and vertical concentration of the wind maximum that is much greater than in either of the other two. The impression left is that the TIROS N section compares rather favorably with the other two in general and lies somewhere between the two in detailing the baroclinic zone.

4.2.3 Upper Midwest Difference Pattern

Returning now to the difference patterns noted previously in the Midwest and particularly the northern Great Plains and extending into southern Canada, we will first briefly consider the off-time effect of the satellite data. Over most of the region the satellite observations were about two hours earlier than the radiosondes and NMC analyses, except in the northwest portion of the region where the satellite analyses were blended with observations that were only 1/2 hour earlier than synoptic time.

For the 1000-500 mb thickness the TIROS N minus NMC analysis difference was positive, indicating the satellite thicknesses were greater and therefore had a higher mean temperature for the layer. Within the area covered by greater than 40 m differences the NMC-analyzed 1000-500 mb thicknesses increased for the 12-hour period bracketing the satellite observations. Thus, allowing for the off-time factor would decrease the NMC-analyzed thicknesses and further increase the differences between the two analyses by an amount varying from 14 percent to 53 percent. However, in the southern Great Lakes and Illinois-Indiana region where the differences were less than 40 m, the off-time factor helps and accounts for up to 100 percent of the differences between the analyses.

The 700-300 mb thickness differences between the two analyses were negative, indicating the satellite mean temperatures for the layer were lower. Within the area covered by greater (negatively) than -50 m differences the NMC-analyzed thicknesses increased for the 12-hour period. Allowing for the off-time factor in this case would decrease the NMC-analyzed thickness values and, therefore, the differences between the two analyses by an amount varying from 14 percent to 55 percent. The largest difference (-92 m), for example, would have 22 percent accounted for by the time change. The largest 12-hour thickness changes account for between 34 percent and 50 percent of the difference between the TIROS N and NMC analyses. Thus, there remain significant differences in these fields to be explored and explained.

To gain an additional feel for the nature of the differences between the two analyses, examine figure 11. It shows profiles of analyzed grid point temperatures at 850 and 500 mb along two lines across the system. The two lines (defined by grid points) start at adjacent grid points near James Bay, Canada, the first one oriented southwestward and the other more westward. One thing to be noted is that the location of the lowest temperatures at the two levels from the NMC analyses changes, i.e., there is an apparent tilt to the cold air, whereas in the TIROS N analyses there is no such tilt. The other feature to be observed is the area of the greatest slope of the temperature profiles. Again, in the profiles from the NMC analyses, the region of the strongest slope changes in location such that the frontal zone exhibits a tilt with height. However, in the TIROS N profiles the area of maximum slope appears not to change location at the two levels. Thus, at least as depicted by conditions at these two levels, the TIROS N analyses show a nearly vertical frontal zone.

To add to the understanding of the manner in which the two types of analyzed thermal patterns differ, figure 12 shows the NMC analysis isentropic cross-section from figure 10 with temperature differences between the TIROS N retrievals and the NMC final analysis superimposed. Generally, the largest differences seen are in the tropopause region where the retrievals are consistently too warm. In the frontal zone, the retrievals show higher temperatures in the lower levels centered toward the cold side and sloping upward along that side of the front. On the other hand, in the mid-troposphere the retrieval temperatures are lower toward the leading or outer side of the frontal zone and tend to slope downward on the warm side of the front. As a result of these temperature differences, the retrievals would, in effect, expand the cold air in the middle levels outward from the cold dome too much and then pull the warmer air in the lower levels inward too far. The net effect of the retrieval temperatures, therefore, is the creation of a frontal zone tending to be too vertical. As an adjunct to this frontal structure, the higher temperatures depicted by the retrievals in the lower levels (relative to the NMC analysis in figure 12) are vertically beneath the lower temperatures in the middle levels resulting in a vertical column that is more unstable than the NMC analysis in the frontal zone. This effect could also be seen in figure 11 where the vertical separation of temperature profiles from the NMC analyses is much less than those from the TIROS N analyses in the frontal region, indicating greater stability.

In order to find the basis of the temperature differences and thermal structure previously discussed, we will next examine some matched retrieval and radiosonde profiles. The radiosondes for International Falls, Minn., and Bismark, N. D., are in figure 13 along with a nearby retrieval for each one. Looking only at the radiosondes one can see the top of the frontal layer rising from near 750 mb at Bismark to about 500 mb at International Falls. The tropopause, with an opposite slope, drops from about 200 mb to near 300 mb. By their nature retrievals lack the vertical resolution to depict a frontal stable layer adequately. Further, however, it can be seen that the retrievals in figure 13 produce a layer that is too warm below the frontal layer and too cold above it. Consequently, the higher the frontal layer, as at International Falls, the greater the depth of the warm layer below it, and

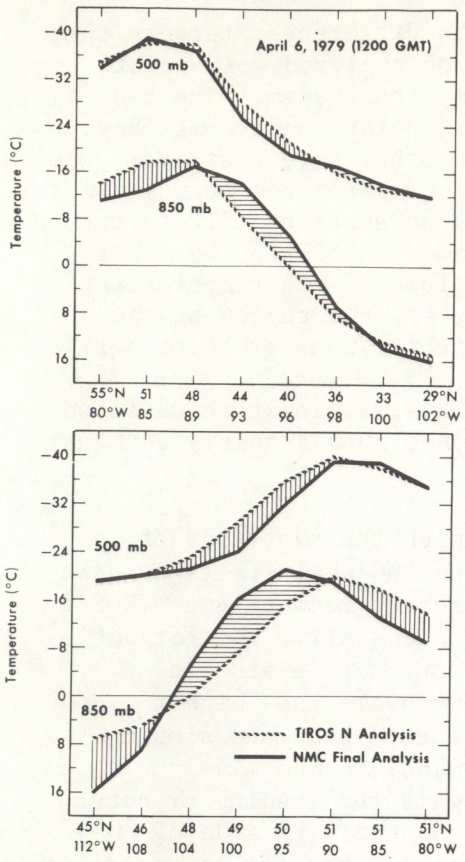

Figure 11.--Analysis temperature profiles along two lines (as given by latitudes and longitudes in figure for 850 mb and 500 mb. NMC analysis in solid lines (1200 GMT) and TIROS N analysis in broken lines (about 1000 GMT) for April 6.

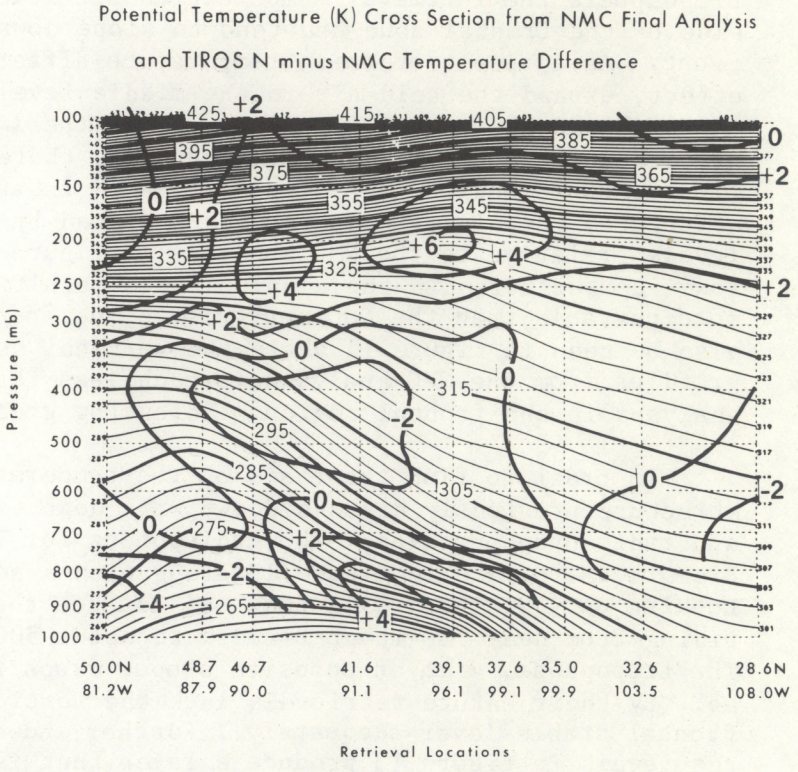

Figure 12.--Isentropic cross-section from NMC analysis (same as fig. 10c) with TIROS N retrieval minus NMC analysis temperature difference superimposed in wide lines (deg. C).

the lower the front the greater the depth of the cold layer above it, as at Bismark. In each case the profile from the retrievals would indicate less stability in the main portion of the troposphere than that shown by the radiosondes. Also, in both cases the indicated tropopause in the retrievals is lower and warmer than the tropopause in the radiosondes.

The retrievals in the previous figure were the cloudy type, whereas in figure 14 are shown to clear retrievals. At Peoria, Illinois, and Topeka, Kansas, the radiosondes again display the frontal slope, from near 700 mb down to below 850 mb at Topeka. The retrieval near Peoria exhibits very similar character to the two previously discussed; too warm below the frontal stable layer and too cold throughout most of the troposphere above it, although the area of the cold region seems to be smaller than in the Bismark comparison, where the front was at a similar height. At Topeka, with the frontal zone considerably lower, the two profiles are quite close through the troposphere. Because of the terrain elevation, the retrieval profile does not extend down far enough to show a layer that is too warm below the front. Again the tropopauses in the retrievals are too low and warm, and the retrieval near Peoria shows less stability than the radiosonde.

Therefore, in these examples of radiosonde and retrieval comparisons one can see the cause of the differences seen earlier in the temperature structure between the NMC analyses and the analyses of satellite-only data. The region of lower temperature shown by the satellite data in the mid-troposphere arises from the lower temperatures above the frontal zone in the vertical profiles; and the higher temperatures below the front give rise to the region of higher temperatures shown by the satellite data in the lower troposphere in the comparison of the analyses. These vertical-profile comparisons also account for the tendency of the satellite depicted frontal zone to be nearly vertical.

4.2.4 Pacific Cyclone

In somewhat of a digression from the primary purpose of the case studies being presented, it is worthwhile to examine the system in the Gulf of Alaska to see how the satellite soundings describe the temperature patterns in comparison with the NMC analyses that were made without benefit of the retrievals. Referring back to figure 7, one recalls the large mature spiral cloud pattern south of the western tip of the Alaskan peninsula, the stage normally associated with a deep, fully-developed cyclone. What are the soundings capable of depicting for such a system?

The system is well covered by retrievals, as seen in figure 6, with cloudy path retrievals associated with the spiral cloud band and clear path outside the cloud band. The data in this area are from 1.3 to 3 hours after synoptic analysis time. What these retrievals show about the thermal structure of the system can be seen in the thickness analyses in figures 8 and 9. The differences between the satellite-only and NMC analyses are quite marked and much larger than those over land. They both show distinct cold centers near 50°N and 160°W, significantly colder and farther east than indicated by the NMC analyses. The thickness ridge associated with the cloud

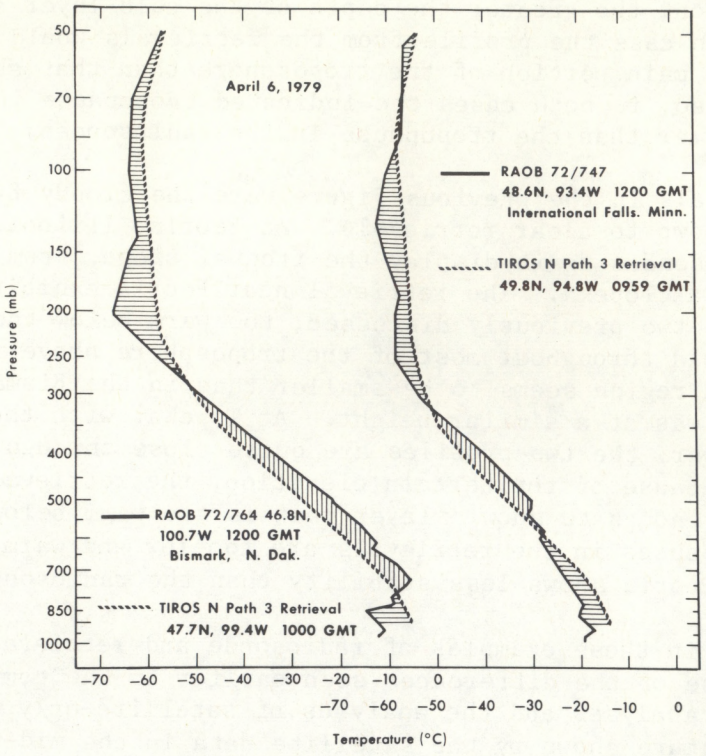

Figure 13.--Radiosonde (1200 GMT) and TIROS N retrieval (about 1000 GMT) pairs for April 6, 1979. Radiosonde temperatures in solid line and retrievals in broken line.

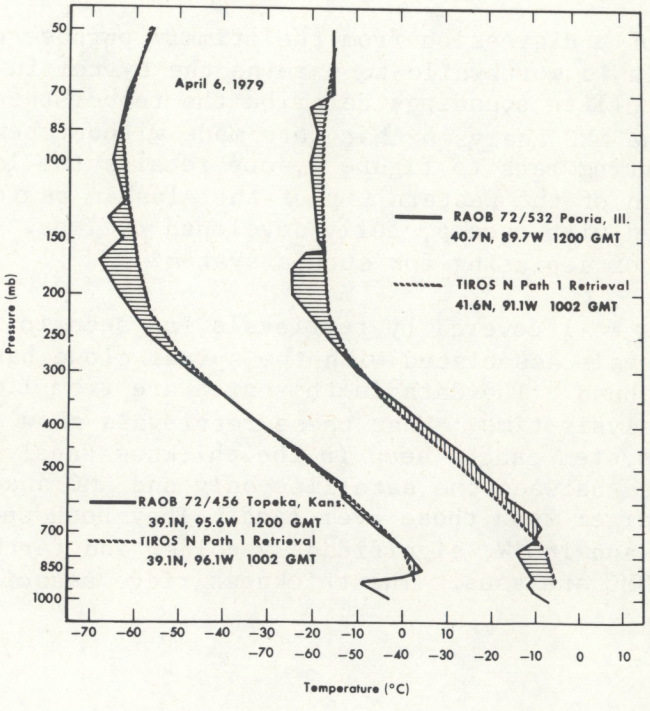

Figure 14.--Same as figure 13.

band has been sharpened and shifted somewhat eastward in the satellite-only analysis. The zone of strongest thermal gradient associated with the jet coming through the trough behind the cloud band has been tightened considerably and shifted southeastward by the satellite data, with an associated increase in cyclonic curvature. In general, therefore, the thermal patterns from the satellite data possess more character than those from the NMC analyses.

Over the ocean, it is difficult to assess the accuracy of the thermal patterns being depicted by the satellite data, but the patterns are in agreement with experience gained from interpretation of satellite cloud patterns as presented by Anderson, et al. (1974). In this regard, one should note the placement of the thickness ridge, region of tightest gradient, and the cold center.

To provide a more complete picture of the 3-dimensional structure, we can use isentropic cross sections once again. The cross sections in figure 15 are taken west-east through the system near 50° N. The one from the TIROS N data shows a distinct frontal zone between approximately 145° and 150° W with a clearly defined thermal wind maximum centered at 300 mb. In the NMC analysis cross-section there is a rather weak baroclinic zone in the mid-troposphere with only a very weak thermal wind maximum. The frontal zone in the TIROS N section does appear to be nearly vertical, which may be a drawback in light of the preceding discussion of results from the frontal zone in the midwest.

North-south cross sections through this system (not shown) using the TIROS N data and the NMC analyses were in much better agreement, indicating that the meridional temperature gradients in the NMC analyses were probably defined more realistically.

There is one location on the cross section in figure 15 that can be checked at ship P located at 50°N and 145°W. The 1200 GMT radiosonde and the TIROS N retrieval closest to that location are shown in figure 16. An occluded front (cold type) was west of ship P so that the stable layer centered near 850 mb in the radiosonde was the warm front ahead of the occlusion. The retrieval displays the usual pattern of being too warm below the stable layer and for some distance into the relatively stable lower part of the radiosonde, then becoming too cold above that point through the middle troposphere. The tropopause in the retrieval is characteristically too low and warm. The net result of the above is that the 1000-500-mb thickness of the two profiles agrees very well but the 700-300 mb TIROS N thickness is too small. Despite this slight disagreement, one cannot help but feel that the TIROS N data in this case are displaying thermal structure and other information that are lacking in the NMC analysis.

4.3 Case Study - December 12, 1979, 0000GMT

4.3.1 Synoptic Situation

On December 12, there was a rather strong cold frontal zone through the midwestern United States. It extended southwestward from a 1004 mb surface

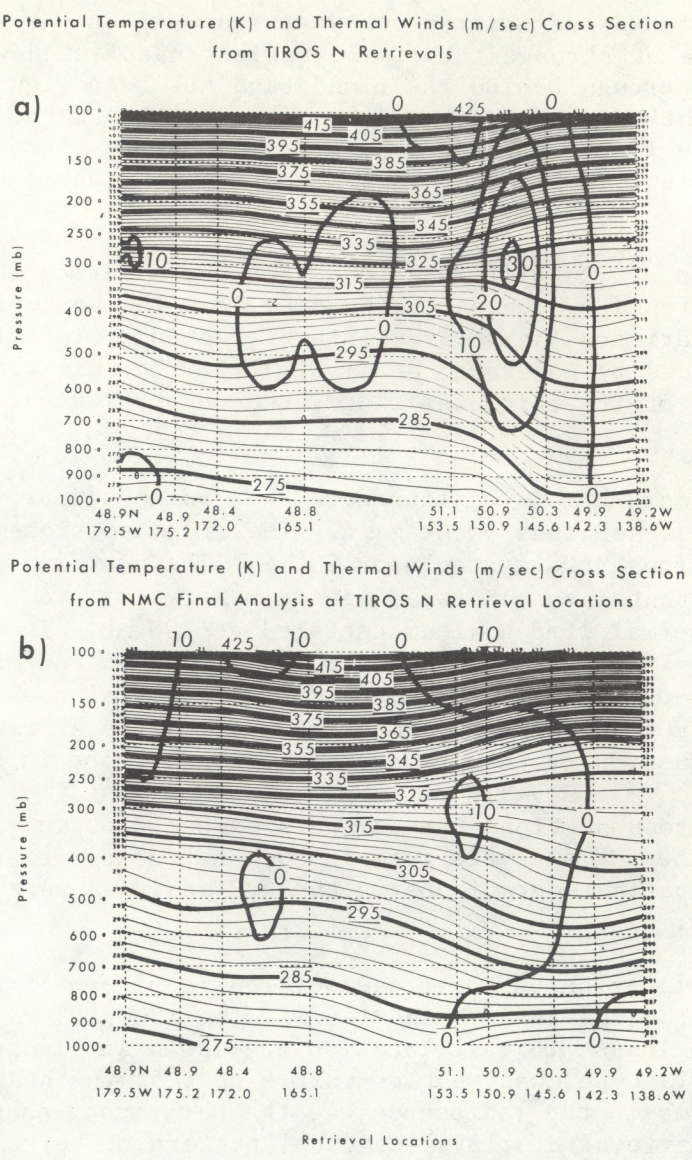

Figure 15.--Isentropic cross sections for 1200 GMT April 6, 1979 (TIROS N about 1330 to 1500 GMT). Potential temperature (deg. K) in narrow solid lines and thermal winds in wide solid lines (m/sec). a) TIROS N retrievals, and b) NMC final cycle analysis at TIROS N locations.

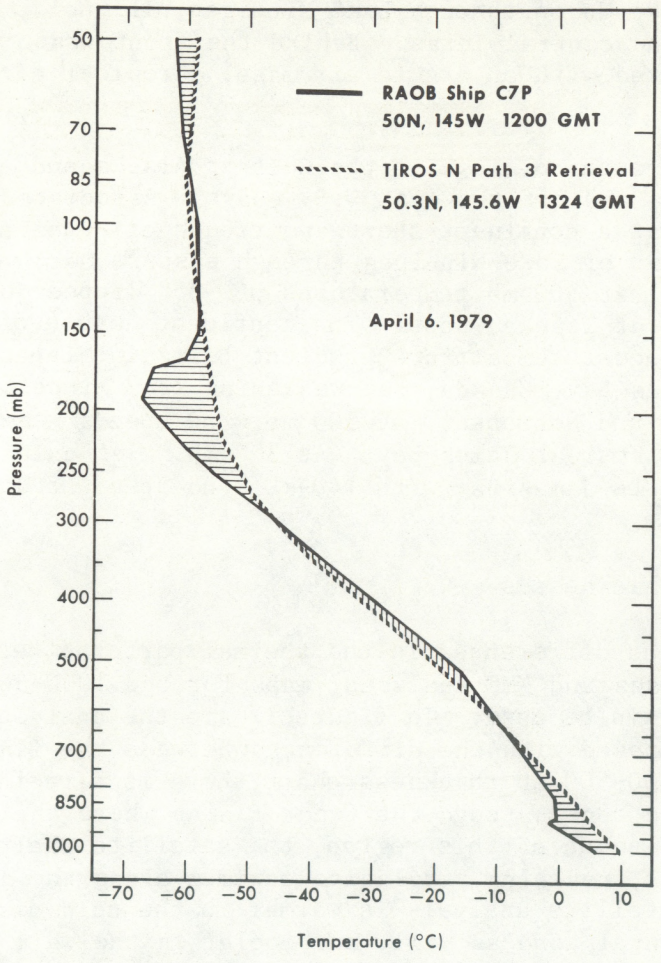

Figure 16.--Radiosonde for ship P, 1200 GMT April 6, 1979 (solid line) and nearby TIROS N retrieval, 1324 GMT (broken line).

low just north of Lake Huron through Lake Michigan, Illinois, Missouri, northwest Arkansas and central Texas. Behind the front was a 1030 mb high in South Dakota associated with an arctic air mass. Tropical air was entering south Texas.

Aloft there was a sharp ridge in the Gulf of Alaska and a broad ridge in eastern North America and off the east U.S. coast. Associated with the surface cold front was a confluent shortwave trough oriented northeast-southwest running east of Lake Winnipeg through eastern North Dakota and Utah to southern California. At 500 mb temperatures of -35° dipped just into North Dakota but were -15° at Topeka, Kans. The confluent nature of the trough resulted in the strongest temperature gradient being in Minnesota and northeastward to James Bay, Canada, but weakening from Minnesota southwestward through South Dakota and Nebraska. At 500 mb wind speeds were 85 kts. at St. Cloud, Minn., and 100 kts. at James Bay. At 300 mb a jet axis extended from southeastern Arizona to James Bay with 140-kt wind speed at James Bay and 120 kts at St. Cloud.

4.3.2 Analyses of Thicknesses

To illustrate the differences in the thermal patterns between the satellite data analyses and NMC analyses, maps for the 1000-500 mb and 700-300 mb thickness will again be used. In figure 17 are the analyses made from TIROS N data superimposed with the differences between the TIROS N and NMC analyses. On the 1000-500-mb thickness chart there is a region in the thermal trough and baroclinic zone through the Great Plains where the TIROS N analysis is warmer. East and south of this region, the satellite analysis is colder than the NMC analysis, reaching a relative maximum along the Texas Gulf coast. Since the satellite analysis is warmer in the cold air and through the rear side of the frontal zone as well, and cooler in the warm air, there is a weakening and some shifting of the 1000-500 mb thickness gradient in the baroclinic region. The actual maxima of negative difference between the two analyses occurs in the higher terrain regions of the western part of the continents, similarly to the situation seen in the first case.

Examining the 700-300 mb thickness analysis, it can be seen that the differences between the two analyses are generally much smaller than in the analysis of the 1000 - 500 mb thickness. Associated with the thermal trough in the northern Great Plains is a region where the satellite analysis is colder than the NMC analysis and centered in the strong gradient ahead of the trough. In addition, the satellite analysis shows the ridge ahead of the trough to be warmer than does the NMC analysis. As in the previous case, the region where the 700-300 mb thickness is smaller is located essentially coincident with the region where the 1000 - 500 mb thickness is larger.

4.4.4 Isentropic Cross Sections

As before, we will examine the 3-dimensional structure more thoroughly through isentropic cross sections. Figure 18 shows the locations of radiosondes and TIROS N soundings used in the cross sections. Three cross sections are shown in figure 19: one from the radiosonde reports, one from

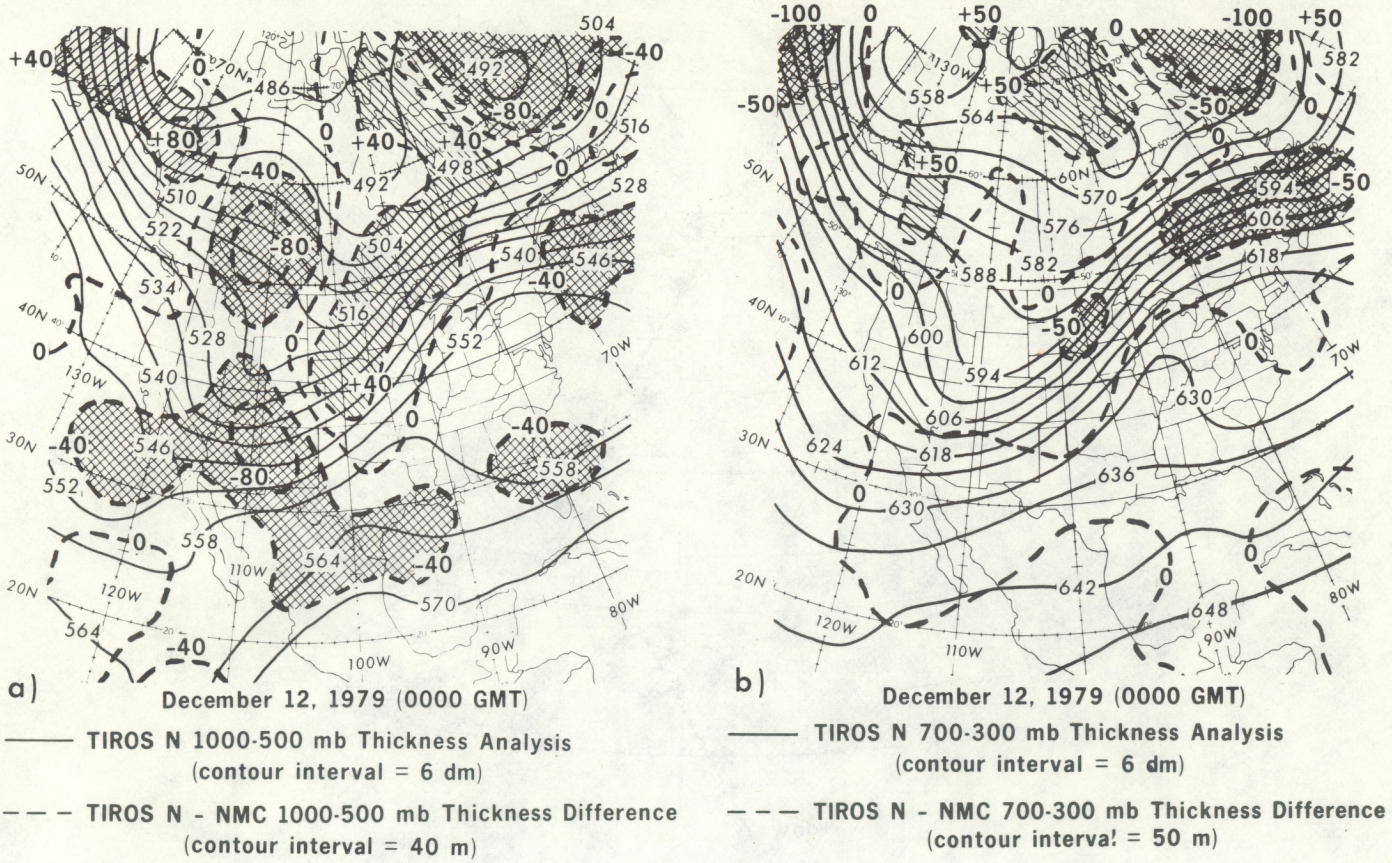

Figure 17.--a) TIROS N 1000 - 500 mb thickness analysis in solid lines (contour interval = 6 dm) and the broken lines are the TIROS N minus NMC analysis thickness difference (contour interval = 40 m) for 0000 GMT December 12, 1979. b) TIROS N 700 - 300 mb thickness analysis with thickness difference the same as a) except contour interval = 50 m.

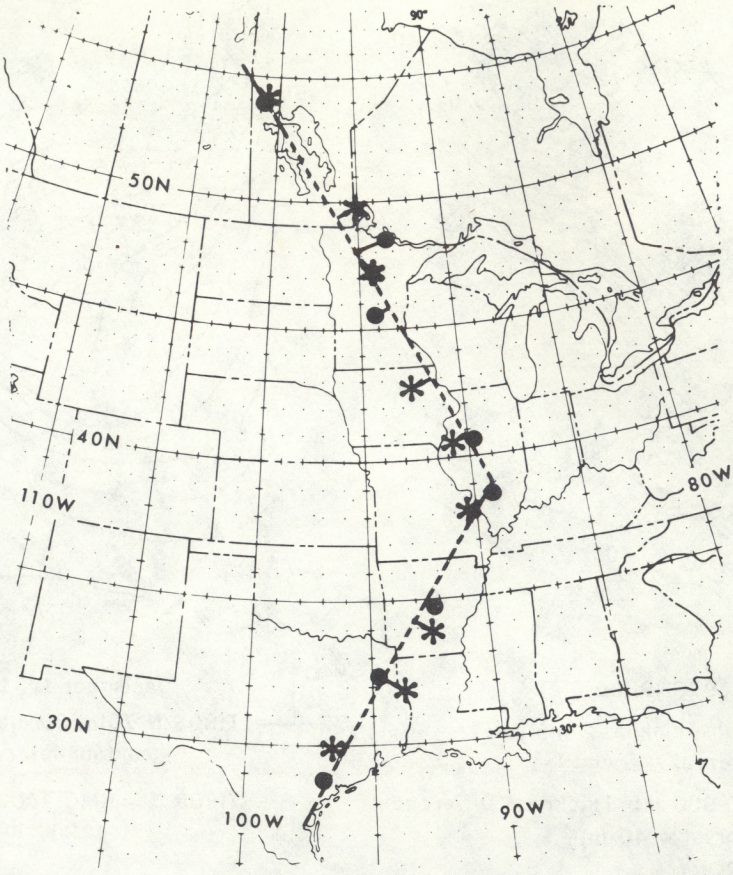

Figure 18.--Locations of radiosondes (solid circles) for 0000 GMT December 12, 1979 and TIROS N retrievals (stars) about 2100 GMT December 11, used in cross sections in figure 19. Locations are projected onto broken line that serves as the base axis for figure 20.

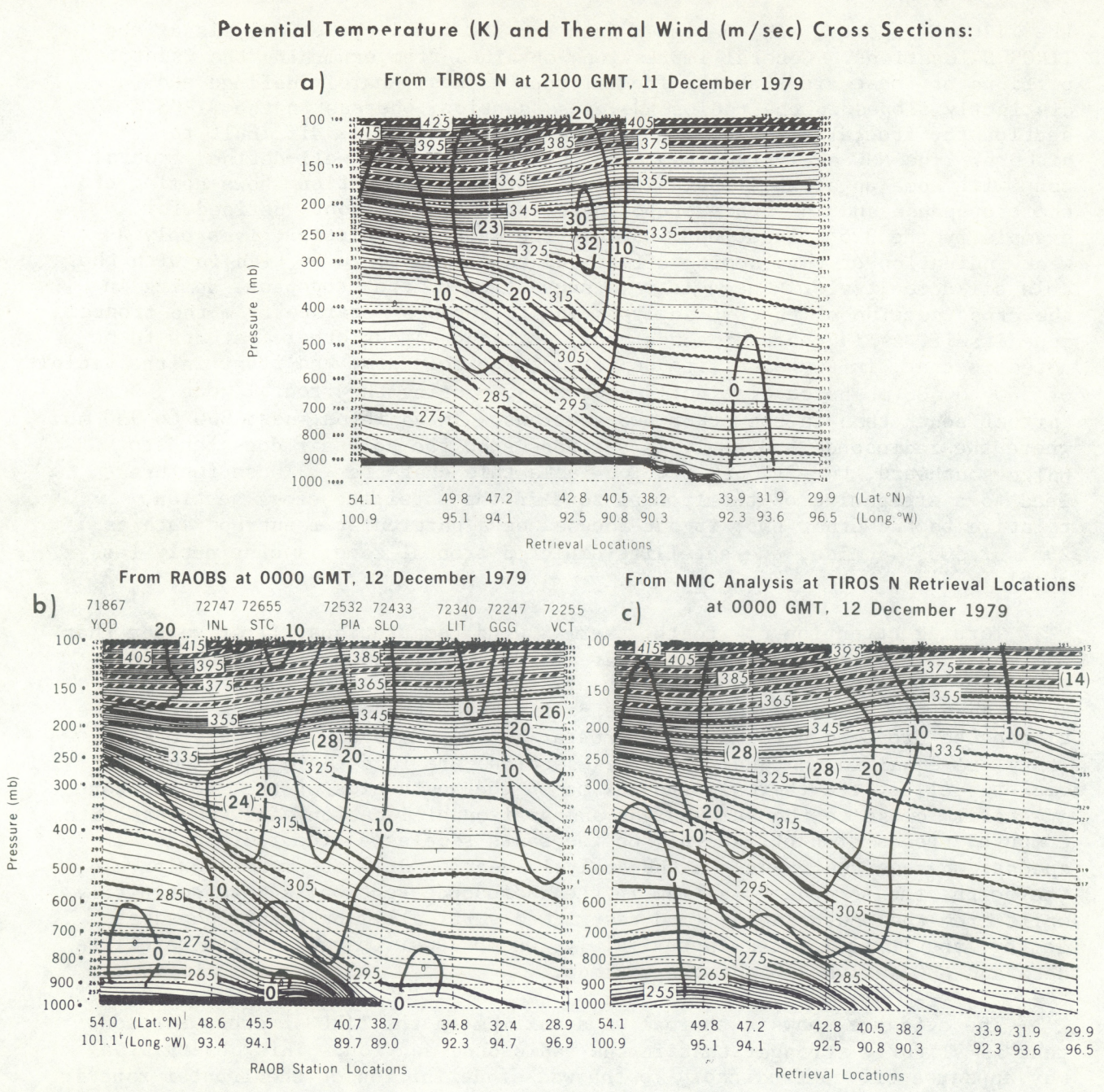

Figure 19.--Isentropic cross-sections for 0000 GMT December 12, 1979 (TIROS N about 2100 GMT December 11). Potential temperature (deg. K) in narrow solid lines and thermal winds in wide solid lines (m/sec). a) TIROS N retrievals; b) radiosondes; and c) NMC final cycle analysis at TIROS N locations.

the TIROS N reports, and one taken from the NMC final-cycle analysis at the TIROS N locations. General impressions obtained from examining the isentropic portions of these are that the frontal zone is most sharply defined and distinctly sloped in the radiosonde cross section, whereas in the TIROS N section the frontal zone appears broader and the slope is difficult to discern. The NMC analysis cross section shows a fairly well-defined frontal zone with some apparent slope. The radiosonde cross section shows doming of the tropopause and the upper troposphere south of the front, defined for example by the 325°K isentrope, whereas the satellite section gives only a weak indication of this doming effect, and that appears to be tied in with the cold air dome itself. There is some suggestion of the tropopause doming in the cross section of the NMC analyses and it appears separate from the frontal zone itself, as in the radiosonde cross section. Among other features to be noted is that, in the satellite depiction, the cold dome and front in the vicinity of 500 to 400 mb bulge distinctly southward, placing the frontal zone farther south than in the other two sections. In addition, near 800 to 900 mb where the radiosonde and analysis sections show the cold air does tend to bulge southward, the TIROS N section lacks this character. These features lead to a steepening of the frontal zone in the satellite cross section, relative to the other two, if one focuses on a particular isentrope such as 295° or 305°K. Also, the satellite depicted frontal zone is distinctly less stable.

Turning attention now to the thermal wind computations, first we see that the maximum wind speed is actually greater in the TIROS N section than in either of the others. The maxima in all three sections are located farther south than the expected location, which is at the tropopause break (where the tropopause drops down to meet the frontal zone). However, secondary maxima (they are equal in the analysis cross section) are located in the expected region. All of the thermal wind maxima on the south side of the frontal zone are fairly close to the same height and horizontal location, and the satellite computed speeds drop off sharply on the south side as do the radiosonde speeds, whereas the speeds in the analysis section drop off more slowly. To the north, the secondary maximum in the radiosonde section is more definitely split from the southern one (and restricted vertically) by the tropopause doming, and it is located approximately 100 mb lower than where the satellite data and NMC analyses place the maximum.

The evidence shows a thermal wind maximum in the TIROS N cross section that is slightly stronger than in the radiosonde section. This observation may appear a bit contradictory to the weaker definition of the frontal zone in the TIROS N analysis; however, the thermal winds are accumulated vertically and, since the satellite soundings place most of the tropospheric temperature gradient in a vertically oriented column rather than a sloping zone as in the radiosondes, the net effect on the thermal winds is comparable. This suggests that the thickness gradients through the depth of the troposphere in the satellite soundings are representative of the atmosphere.

4.3.4 Differences in Temperature Structure

Earlier it was shown that in the satellite analysis a colder region overlaid a warmer layer. This effect was also noted in the examination of the cross sections. To study this structure closer, figure 20 shows the 850 mb and 500 mb temperature profiles along the line of the cross section. The line is shown in figure 18, and the radiosonde and satellite locations are projected normally onto the common line so that the profiles may be superimposed. This was not possible in the cross sections, because the radiosondes and satellite retrievals are not collocated. In figure 20, the radiosonde profiles are shown as a solid line, and the satellite profiles are shown with a broken line. The NMC analysis values are shown with a triangle for both the retrieval and radiosonde locations. At 850 mb, the 1000 - 500 mb difference patterns pointed out earlier stand out quite clearly. The analysis points follow the radiosonde profile in reasonable agreement; however, the retrieval profile shows clearly the higher temperatures on the cold side of the baroclinic zone and the lower temperatures on the warm side of it. This results in a definite weakening of the temperature gradient in the frontal zone. At 500 mb the profile differences are not nearly so sharp, but there is a tendency for the satellite temperatures to be lower in the same region where they are higher at 850 mb, and higher at 500 mb where the temperatures at 850 mb were lower. These profiles help clarify the differences in temperature structure in the baroclinic zone between that measured by the radiosondes and that depicted by the satellite retrievals. In this case there are no collocated radiosonde and retrievals in the baroclinic zone so that the vertical profiles could vividly illustrate the differences in the temperature structure as they did in the first case presented. However, it is clear from figure 20 that the satellite displays much less stability in the northern end of the baroclinic zone, although greater stability is shown by the satellite data over that reported by the radiosonde data in the southern portion of the baroclinic zone. Nowhere do the satellite soundings display as much stability as the radiosondes. Again, while these results are not unexpected, given the nature of the two measurements, they illustrate the horizontal synoptic-scale effects produced by these differing measurements of the vertical temperature structure.

4.4 Case Study - May 6, 1980, 1200 GMT

4.4.1 Synoptic Situation

The surface map for this situation shows a large 1036-mb high center in north-western Canada and a 999-mb low center at the northeast end of Lake Ontario with only weak circulation about it. A cold front extends from the low center through western New York, Ohio, and through the southern parts of the states of Indiana, Illinois, Missouri, and Kansas. In the midwest, the front was rather old with weak temperature and pressure gradients associated with it. This front was associated with a maritime air mass, and it was apparent from the surface temperatures that by this time some arctic air had infiltrated the northern Great Plains and midwest, although there was no longer an identifiable front.

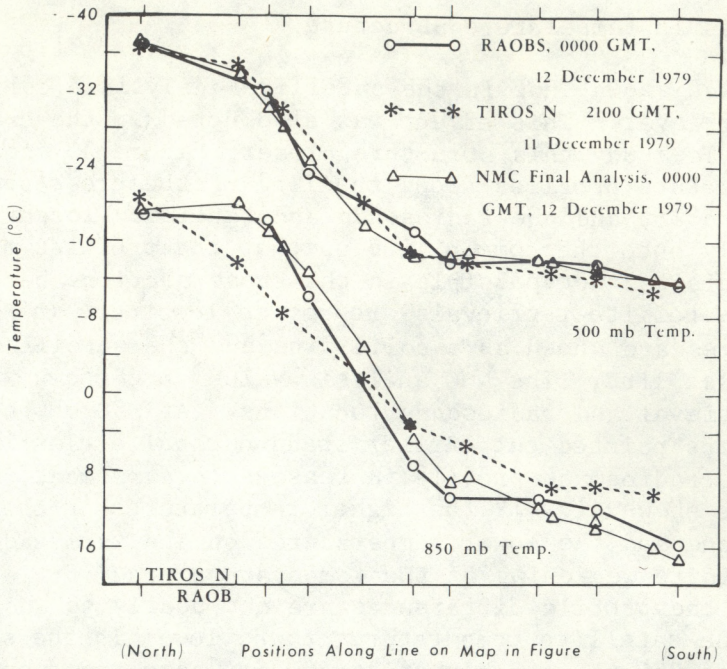

Figure 20.--Temperature profiles for 850 mb and 500 mb with positions along base line taken from figure 18. Radiosonde temperatures shown with open circles and solid line, TIROS N retrieval temperatures with stars and broken line, and NMC analysis temperatures for both radiosonde and TIROS N locations, with triangles and thin solid line.

In the upper air there was a long wave trough off the west coast and a ridge in the western part of North America. A short wave trough with a difluent contour pattern had moved southeastward from northwestern Canada. This configuration of systems placed the strongest winds and gradients of temperature on the southwestern side of the trough, i.e., from the North Dakota region to west of Lake Winnipeg. The jet axis was oriented from west of Lake Winnipeg to between International Falls and St. Cloud, Minn., and to near Green Bay, Wisc. Green Bay had a 300-mb wind speed of 135 kt, and speeds decreased rapidly downstream from there.

4.4.2 Analyses of Thicknesses

The thickness pattern and analyses of the 1000 - 500 mb and 700 - 300 mb layers made from satellite data alone together with the differences between the satellite and NMC final-cycle analyses are shown in figure 21. On the 1000 - 500 mb analysis, the portion of the area of concern that is north of Lake Superior and the Canadian border is a region where the satellite analysis is warmer than the NMC analysis. On the other hand, throughout most of the upper midwest and Great Plains the satellite analysis is colder than the NMC analysis, but by relatively small magnitudes. As a result of the locations of these difference patterns about the baroclinic zone in the upper midwest, the thickness gradient in the satellite analysis is weakened.

The 700 - 300 mb thickness analysis in figure 21 shows a somewhat similar pattern of differences between the satellite-only and NMC analyses. The positive center north of Lake Superior denotes an area where the satellite analysis is warmer in the pool of cold air at middle and upper levels. Much of this same area was also warmer in the lower levels, as seen above. The axis of negative differences in thickness in the upper midwest shows the satellite analysis to be even colder in upper levels than in lower. This pattern indicates that the cold air in the middle and upper troposphere would tend to be expanded southwestward, and also the thickness gradients in the upper midwest would be somewhat weakened over those in the NMC analysis.

4.4.3 Isentropic Cross Sections

Isentropic cross sections across the baroclinic zone from the satellite retrievals, radiosondes, and the NMC final analysis are shown in figure 23 and will again be used to facilitate comparison of the three-dimensional thermal structure. The locations of the radiosondes and NOAA 6 soundings used in the cross sections are shown in figure 22. The northern two NOAA 6 retrievals were cloudy type while the remainding ones were clear. First of all, inspecting the cross section taken from the radiosondes, it appears that the frontal zone is non-typical in that there is no deep unified frontal zone. The upper level frontal zone is confined to the region above 600 mb (north of Omaha), up to the tropopause, and the surface front analyzed through southern Kansas appears only weakly above the surface. The arctic air shows up possibly as a shallow stable layer north of Omaha which then slopes upward north of St. Cloud to a dome in the vicinity of International Falls. The result is an irregular, broad, essentially vertical baroclinic zone between

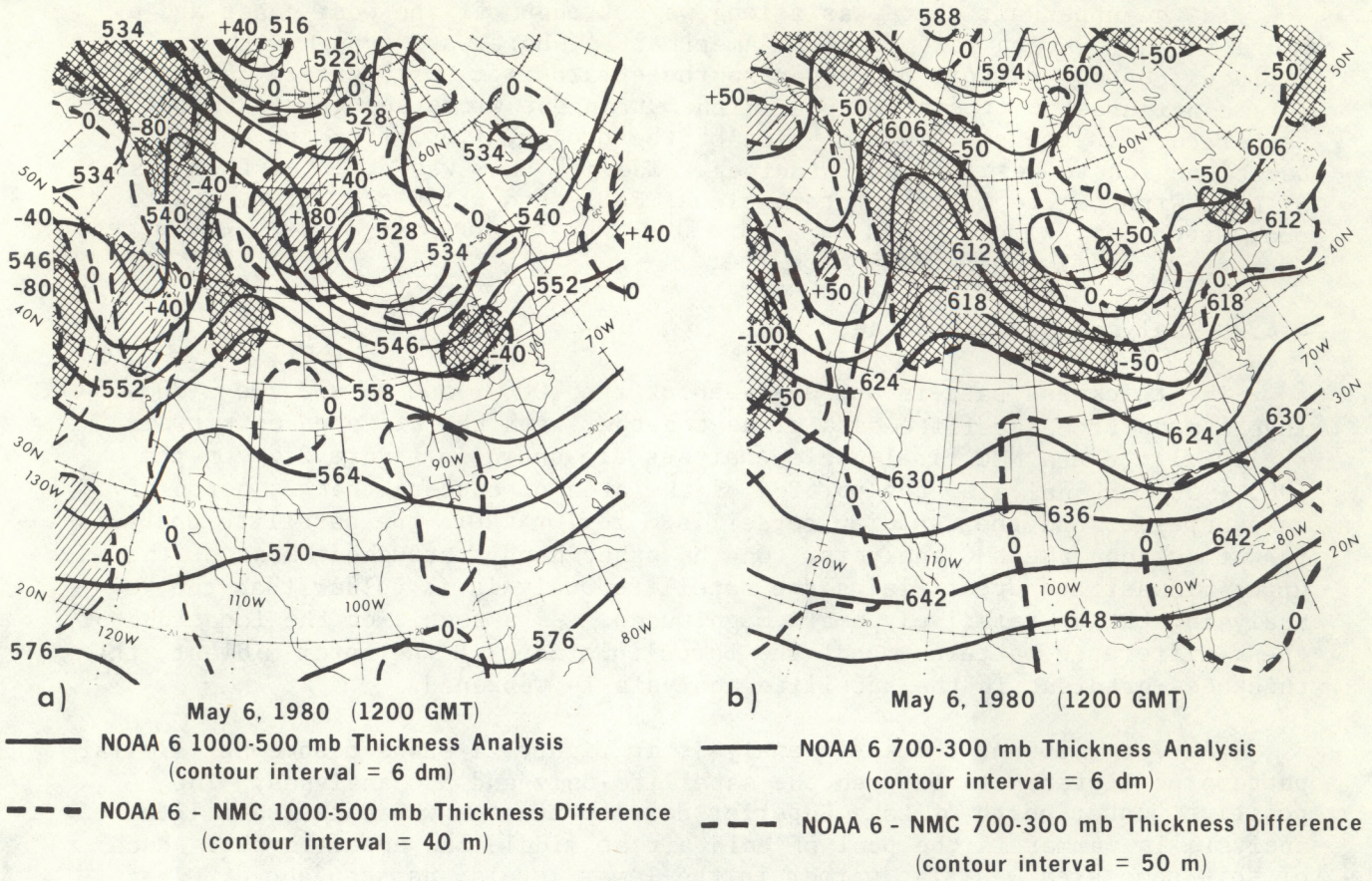

Figure 21.--a) NOAA 6 1000 - 500 mb thickness analysis (about 1400 GMT) in solid lines, and in broken lines the NOAA 6 minus analysis thickness difference for 1200 GMT May 6, 1980; b) NOAA 6 700 - 500 mb thickness analysis with thickness difference the same as a). Contour intervals the same as figure 17.

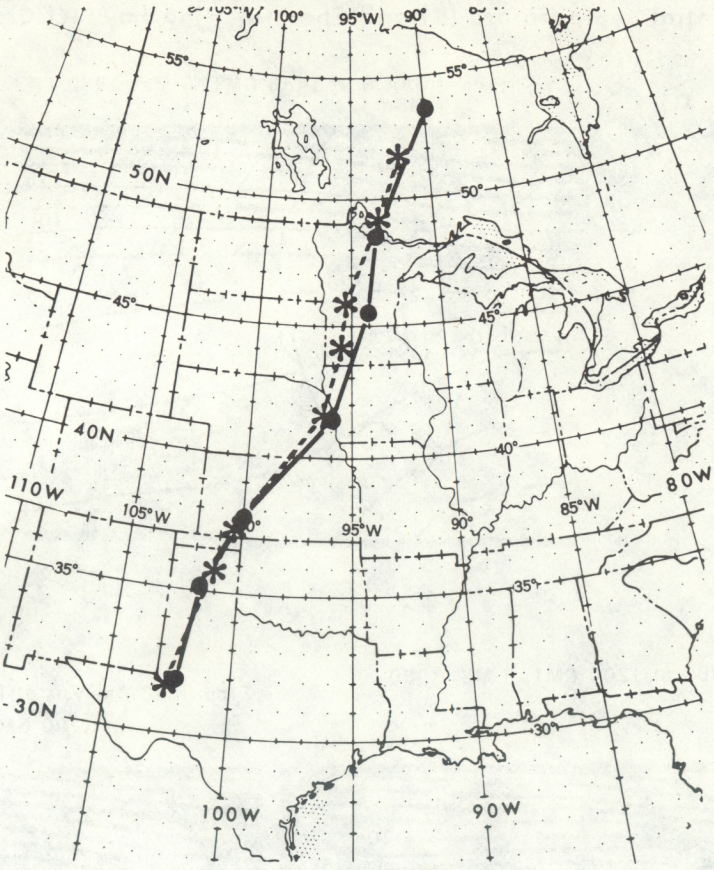

Figure 22.--Locations of radiosondes (solid circles) for 1200 GMT May 6, 1980 and NOAA 6 retrievals (stars), about 1400 GMT, used in cross sections in figure 23.

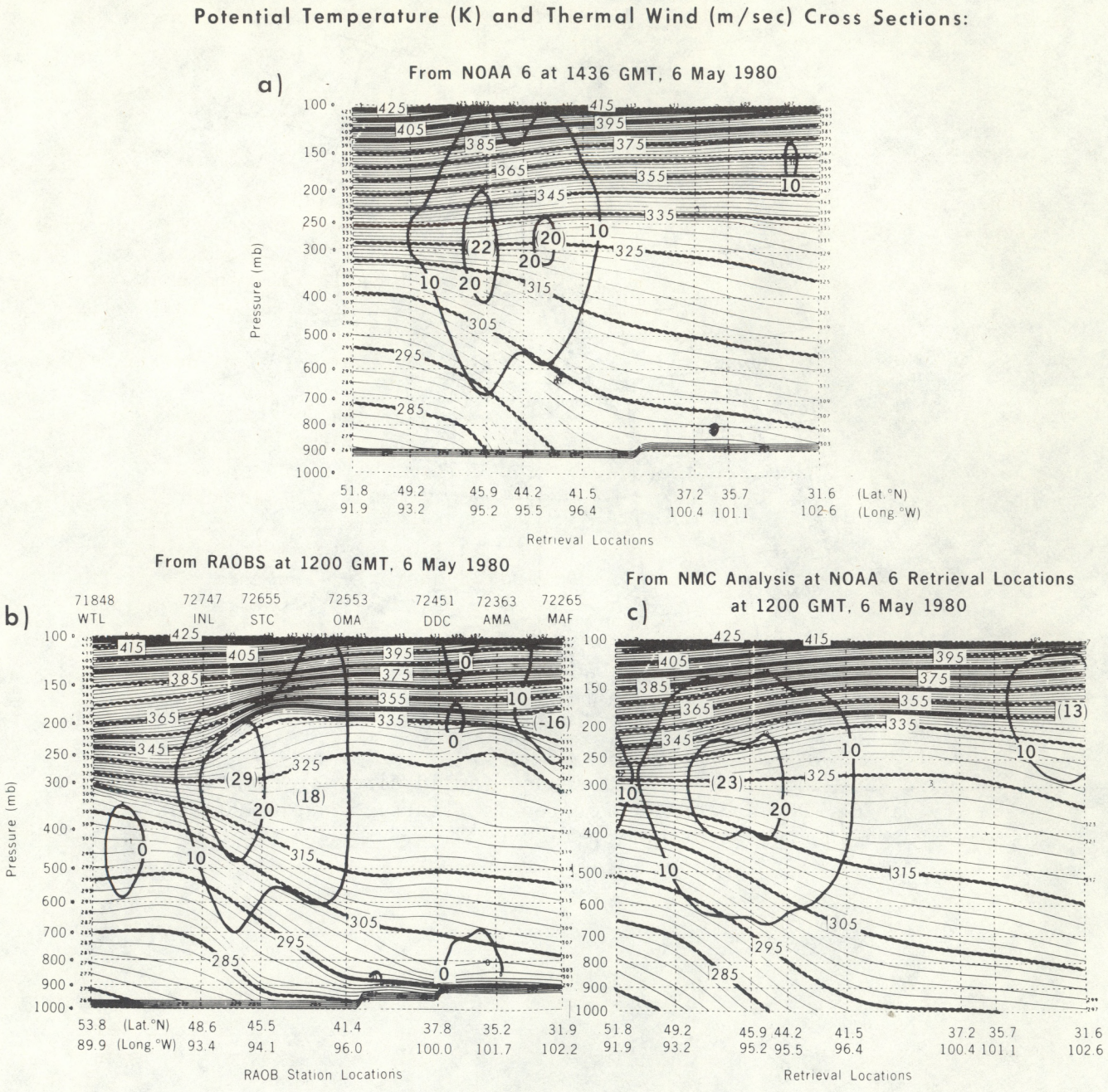

Figure 23.--Isentropic cross-sections for 1200 GMT May 6, 1980 (NOAA 6 about 1400 GMT). Same as figure 19.

Omaha and International Falls up to 500 mb, above which the zone slopes northward up to around 350 mb north of International Falls.

As would be expected, the details of the thermal structure disclosed in the radiosonde cross section are lacking in both the satellite and analysis versions. The cross section derived from the satellite retrievals typically displays an essentially vertical baroclinic zone in approximately the same latitude band as the radiosondes but extending the entire depth to the tropopause, whereas the analysis cross section does suggest a sloping character above 500 mb. The doming in the tropopause at St. Cloud in the radiosonde cross section is absent in the satellite depiction, and south of this point the tropopause is indicated about 50 mb lower than the radiosondes show. The analysis section has a tendency to dome the tropopause farther south than the radiosondes but does bring it up to about the same height.

The colder leading edge of the baroclinic zone seen in the satellite analysis (fig. 21b) is discernible in the satellite cross section as a southward bulge of the frontal zone above 500 mb. This phenomenon also accounts for the lack of slope in the satellite frontal zone in the upper troposphere. There is a very slight hint of a bulge in the upper frontal zone region in the analysis section as well, but nothing of the sort is seen in the radiosonde cross section. This equatorward expansion of the cold air in the upper troposphere is typical of the satellite analysis as noted in previous cases.

Further examination of the cross sections reveals that the satellite analysis is somewhat warmer in the 900 - 700 mb region around Omaha and northward than is the radiosonde analysis. On the other hand, the analysis cross section is even warmer in that region than either of them. This relationship between the three accounts for the satellite 1000 - 500 mb thickness analysis appearing colder than the NMC analysis (fig. 21a), when in fact the cross sections show that the satellite retrievals are warmer than the radiosondes. Thus, the type of temperature structure relationship in the baroclinic zone seen in the previous cases is preserved after all, because here the satellite thicknesses are greater in a lower layer coincident with a colder higher layer.

The thermal wind speeds on the cross sections show that the radiosonde maximum is somewhat stronger than the satellite and that it is located very slightly farther north. The maximum in the NMC analysis is about the same strength as the satellite but located slightly farther north also. The heights of the maxima are about the same in all three sections. The satellite soundings give a somewhat broader maximum than either of the other two, especially in the radiosonde section, where the tropopause doming restricts the speed maximum in the vertical and somewhat in the horizontal. Once again the integrated vertical effect of the temperature gradients in the satellite data provide a good representation of what is seen in the radiosonde or analysis cross sections.

4.4.4 Differences in Temperature Soundings

Two of the NOAA 6 soundings in the cross sections are collocated with the Omaha, Neb. and St. Cloud, Minn. radiosondes. These two pairs of soundings are shown in figure 24 and illustrate graphically the points discussed above in the cross sections. The base of the upper level front can be seen in the radiosondes sloping from near 600 mb at Omaha up to 475 mb at St. Cloud. The surface inversion at Omaha is probably evidence of the slightly cooler and dryer air mass, although it is difficult to distinguish it from a normal nocturnal inversion. At St. Cloud this cooler air mass may be associated with the slightly stable layer just above 700 mb up to 570 mb. The intrusion of Arctic air may be evidenced by the lower stable portion of the radiosonde profile. At Omaha, the NOAA 6 retrieval is clearly somewhat warmer in the lower portion of the troposphere up to the upper frontal inversion and then colder above up to nearly 300 mb. This structure agrees with the situation seen in the previous cases, describing how the satellite soundings depict a more nearly vertical frontal zone by being warmer in the cold air below the frontal surface and colder above. The retrieval profile is definitely warmer than the raob in the tropopause region. Near St. Cloud the satellite retrieval, being deeper into the colder air than Omaha, agrees with the radiosonde up to just above 500 mb. Above this level up to 300 mb the retrieval is colder, with once again the warmer tropopause region above 300 mb. This comparison, along with the one at Omaha, demonstrates the source of the colder region in the mid- to upper troposphere in the satellite soundings and explains the apparent bulging of cold air in the satellite cross section toward the warm side of the frontal zone.

4.5 Summary

In these case studies, analyses of the 1000 - 500 mb and 700 - 300 mb thicknesses were made from satellite retrieval data only and compared with the final-cycle NMC analyses (which had no satellite data over land). The satellite data provided patterns that generally compared well with those from the NMC analyses; however, certain characteristic differences in the vicinity of strong baroclinic zones emerged. In these regions, positive differences (satellite warmer than NMC analysis) between the two 1000 - 500 mb thickness analyses were approximately collocated with negative differences between 700 - 300 mb thicknesses.

The nature of the differences in the three-dimensional temperature structure was examined in more detail using isentropic cross sections taken approximately normal to the baroclinic zones. These cross sections were computed separately from satellite retrievals, radiosondes, and from the NMC-analyzed temperatures. The potential temperature gradients were assessed using vertically accumulated thermal windspeeds. The results indicated that the satellite data produced less sharply defined frontal zones than did the radiosondes, although they (satellite) were comparable to the frontal zones produced from the NMC-analyzed fields. Moreover, the frontal zones described by the satellite data tended to be more vertical, which also reduced the stability in the frontal zone itself. The tendency toward a vertical frontal tilt arose because the satellite data spread the cold air in the mid-

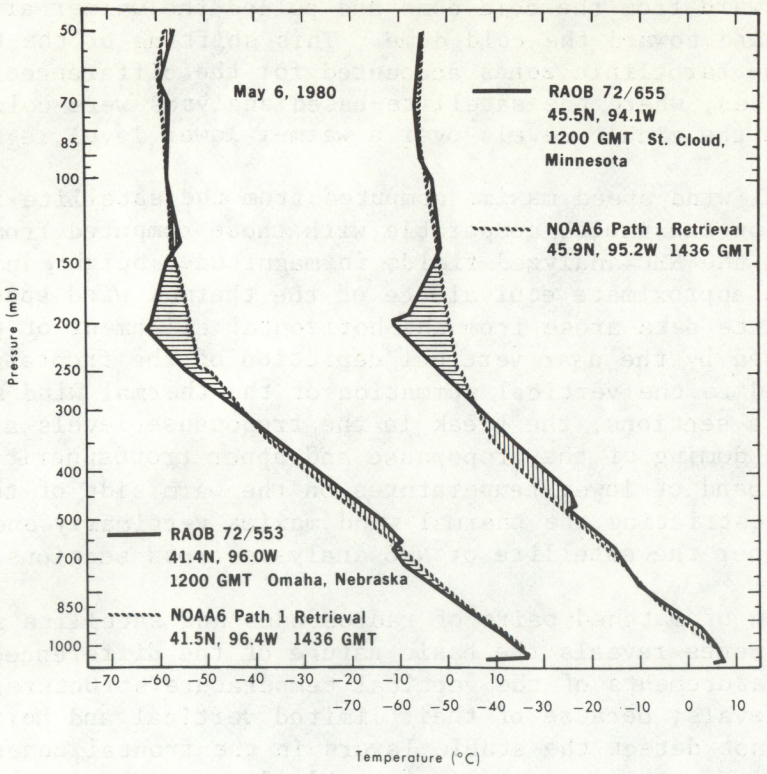

Figure 24.--Radiosonde (1200 GMT) and NOAA 6 retrieval (1436 GMT) pairs for May 6, 1980. Radiosonde temperatures in solid line and retrievals in broken line.

troposphere outward from the cold dome and pulled the warmer air in the lower troposphere inward toward the cold dome. This shifting of the temperature gradients in the baroclinic zones accounted for the differences seen in the thickness analyses, where the satellite-based analyses were colder than the NMC analyses in the middle levels over a warmer lower level region.

The thermal wind speed maxima computed from the satellite retrieval cross sections were, on the whole, comparable with those computed from the radiosondes and the NMC-analyzed fields in magnitude, height, and horizontal location. This approximate equivalence of the thermal wind speeds computed from the satellite data arose from the horizontal alignment of the temperature gradients, caused by the near vertical depiction of the frontal zone, which then contributed to the vertical summation of the thermal wind speeds. In the radiosonde cross sections, the break in the tropopause levels at the wind maximum and the doming of the tropopause and upper tropospheric temperatures (produced by a band of lower temperatures on the warm side of the jet) contribute to restricting the thermal wind maxima vertically and horizontally relative to either the satellite or NMC analysis cross sections.

Examination of matched pairs of radiosondes and satellite soundings in the baroclinic zones reveals the basic nature of the differences between the two types of measurements of the vertical temperature structure. The satellite retrievals, because of their limited vertical and horizontal resolution, do not detect the stable layers in the frontal zones, so that the satellite soundings are warmer below a stable layer and colder above it relative to radiosonde temperatures.

The preceeding comparison between the two sets of measurements thus accounts for the near vertical fronts in the satellite retrieval cross sections and the pattern of differences found between the thickness analyses of satellite data and the NMC analyses. Therefore, what might at first be regarded as merely a limitation in the satellite's ability to measure detailed vertical structure has been shown to result in synoptic-scale horizontal temperature differences. However, the conclusion from the thermal wind speeds in the cross sections is that, taken through the depth of the troposphere, the satellite soundings provide about the appropriate amount of temperature gradient to account for the thermal wind speed maxima.

The earliest case study (which was before the time NMC started using the TIROS N soundings in their analyses) included a strong cyclonic system in the Gulf of Alaska. The analyses from the soundings showed a substantially more intense system with much greater baroclinicity in the temperature structure than did the NMC analyses. This case clearly demonstrated that, despite the limitations described above, the satellite soundings are capable of providing very significant information over oceanic regions, where other types of observations are limited.

Acknowledgements

The authors extend their gratitude to Robert Ryan for his very competent preparation of the figures and to Carroll Maunder for typing the manuscript.

5. References

Anderson, Ralph K. et. al., "Application of meteorological satellite data in analysis and forecasting," ESSA Technical Report, NESS 51, Washington, D.C., Mar. 1974, 330 pp.

Grody, N., "Memo for the record", NESS, Feb. 8, 1979.

Gruber, A., Brodrick, H., and Watkins, C., "Evaluation of sounding data obtained from TIROS N and NOAA 6," Proceedings of the International Conference on Preliminary FGGE Data Analysis and Results, Bergen, Norway, June 23-27, 1980, in press.

Phillips, N., McMillin, L., Gruber, A., and Wark, D., "An evaluation of early operational temperature soundings from TIROS N", Bulletin Amer. Meteor. Soc. Vol. 60, No. 10, Oct. 1979, pp. 1188-1197.

Shapiro, M. A., and Hastings, J. T., "Objective cross-section analyses by Hermite polynomial interpolation on isentropic surfaces", Journal of Applied Meteorology, Vol. 12, No. 5, Aug. 1973, pp. 753-762.

Smith, W., Woolf, H., Hayden, C., Wark, D., and McMillin, L., "The TIROS N Operational Vertical Sounder," Bull. Amer. Meteor. Soc. Vol. 60, No. 10, Oct. 1979, pp. 1177-1187.

FIGURES

1. TIROS N Operational Vertical Sounder (TOVS) weighting functions (normalized).

2. RMS differences between satellite retrieval and radiosonde layer mean temperatures for 30° - 60°N. Hatching indicates RMS values greater than 2°. a) TIROS N over land, b) NOAA 6 over land.

3. Same as figure 2. a) TIROS N over sea; b) NOAA 6 over sea.

4. Mean differences between satellite retrieval and radiosonde layer mean temperatures for 30° - 60°N. Hatching indicates mean difference values greater than 1° (+ or -). a) TIROS N over land, b) NOAA 6 over land.

5. Same as figure 4. a) TIROS N over sea; b) NOAA 6 over sea.

6. TIROS N retrieval locations for April 6, 1979. Broken lines delineate orbital swaths with times as indicated. Open circles indicate clear path, stars indicate partly cloudy path, and solid circles indicate cloudy path retrievals.

7. TIROS N digitized infrared mosaic for April 6, 1979. Time corresponds to swaths in figure 6.

8. a) NMC 1000 - 500 mb thickness analysis in solid lines (contour interval = 6 dm), and the broken lines are the TIROS N minus NMC thickness difference (contour interval = 40 m) for 1200 GMT, April 6, 1979. b) TIROS N 1000 - 500 mb thickness analysis in solid lines (contour interval = 6 dm) with broken lines same as a) for about 1000 GMT April 6, 1979.

9. a) Same as figures 9a) and b) except for the 700 - 300 mb thickness, and the thickness difference contour interval = 50 m.

10. Isentropic cross-sections for 1200 GMT April 6, 1979 (TIROS N about 1000 GMT). Potential temperature (deg. K) in narrow solid lines and thermal winds in wide solid lines (m/sec). a) TIROS N retrievals, b) radiosondes, c) NMC final cycle analysis at TIROS N locations, and d) TIROS N locations indicated with triangles and broken line, radiosonde locations with circles and solid line.

11. Analysis temperature profiles along two lines (as given by latitudes and longitudes in figure) for 350 mb and 500 mb. NMC analysis in solid lines (1200 GMT) and TIROS N analysis in broken lines (about 1000 GMT) for April 6.

12. Isentropic cross-section from NMC analysis (same as fig. 10c) with TIROS N retrieval minus NMC analysis temperature difference superimposed in wide lines (deg. C).

13. Radiosonde (1200 GMT) and TIROS N retrieval (about 1000 GMT) pairs for April 6, 1979. Radiosonde temperatures in solid line and retrievals in broken line.

14. Same as figure 13.

15. Isentropic cross sections for 1200 GMT April 6, 1979 (TIROS N about 1330 to 1500 GMT). Potential temperature (deg. K) in narrow solid lines and thermal winds in wide solid lines (m/sec). a) TIROS N retrievals, and b) NMC final cycle analysis at TIROS N locations.

16. Radiosonde for ship P, 1200 GMT April 6, 1979 (solid line) and nearby TIROS N retrieval, 1324 GMT (broken line).

17. a) TIROS N 1000 - 500 mb thickness analysis in solid lines (contour interval = 6 dm) and the broken lines are the TIROS N minus NMC analysis thickness difference (contour interval = 40 m) for 0000 GMT December 12, 1979. b) TIROS N 700 - 300 mb thickness analysis with thickness difference the same as a) except contour interval = 50 m.

18. Locations of radiosondes (solid circles) for 0000 GMT December 12, 1979 and TIROS N retrievals (stars) about 2100 GMT December 11, used in cross sections in figure 19. Locations are projected onto broken line, that serves as the base axis for figure 20.

19. Isentropic cross-sections for 0000 GMT December 12, 1979 (TIROS N about 2100 GMT December 11). Potential temperature (deg. K) in narrow solid lines and thermal winds in wide solid lines (m/sec). a) TIROS N retrievals; b) radiosondes; and c) NMC final cycle analysis at TIROS N locations.

20. Temperature profiles for 850 mb and 500 mb with positions along base line taken from figure 18. Radiosonde temperatures shown with open circles and solid line, TIROS N retrieval temperatures with stars and broken line, and NMC analysis temperatures for both radiosonde and TIROS N locations) with triangles and thin solid line.

21. a) NOAA 6 1000 - 500 mb thickness analysis (about 1400 GMT) in solid lines, and broken lines are the NOAA 6 minus analysis thickness difference for 1200 GMT May 6, 1980; b) NOAA 6 700 - 500 mb thickness analysis with thickness difference the same as a). Contour intervals the same as figure 17.

22. Locations of radiosondes (solid circles) for 1200 GMT May 6, 1980 and NOAA 6 retrievals (stars), about 1400 GMT, used in cross sections in figure 23.

23. Isentropic cross-sections for 1200 GMT May 6, 1980 (NOAA 6 about 1400 GMT). Same as figure 19.

24. Radiosonde (1200 GMT) and NOAA 6 retrieval (1436 GMT) pairs for May 6, 1980. Radiosonde temperatures in solid line and retrievals in broken line.

(Continued from inside front cover)

NESS 61 The Measurement of Atmospheric Transmittance From Sun and Sky With an Infrared Vertical Sounder. W. L. Smith and H. B. Howell, September 1972, 16 pp. (COM-73-50020)

NESS 62 Proposed Calibration Target for the Visible Channel of a Satellite Radiometer. K. L. Coulson and H. Jacobowitz, October 1972, 27 pp. (COM-73-10143)

NESS 63 Verification of Operational SIRS B Temperature Retrievals. Harold J. Brodrick and Christopher M. Hayden, December 1972, 26 pp. (COM-73-50279)

NESS 64 Radiometric Techniques for Observing the Atmosphere From Aircraft. William L. Smith and Warren J. Jacob, January 1973, 12 pp. (COM-73-50376)

NESS 65 Satellite Infrared Soundings From NOAA Spacecraft. L. M. McMillin, D. Q. Wark, J.M. Siomkajlo, P. G. Abel, A. Werbowetzki, L. A. Lauritson, J. A. Pritchard, D. S. Crosby, H. M. Woolf, R. C. Luebbe, M. P. Weinreb, H. E. Fleming, F. E. Bittner, and C. M. Hayden, September 1973, 112 pp. (COM-73-50936/6AS)

NESS 66 Effects of Aerosols on the Determination of the Temperature of the Earth's Surface From Radiance Measurements at 11.2 m. H. Jacobowitz and K. L. Coulson, September 1973, 18 pp. (COM-74-50013)

NESS 67 Vertical Resolution of Temperature Profiles for High Resolution Infrared Radiation Sounder (HIRS). Y. M. Chen, H. M. Woolf, and W. L. Smith, January 1974, 14 pp. (COM-74-50230)

NESS 68 Dependence of Antenna Temperature on the Polarization of Emitted Radiation for a Scanning Microwave Radiometer. Norman C. Grody, January 1974, 11 pp. (COM-74-50431/AS)

NESS 69 An Evaluation of May 1971 Satellite-Derived Sea Surface Temperatures for the Southern Hemisphere. P. Krishna Rao, April 1974, 13 pp. (COM-74-50643/AS)

NESS 70 Compatibility of Low-Cloud Vectors and Rawins for Synoptic Scale Analysis. L. F. Hubert and L. F. Whitney, Jr., October 1974, 26 pp. (COM-75-50065/AS)

NESS 71 An Intercomparison of Meteorological Parameters Derived From Radiosonde and Satellite Vertical Temperature Cross Sections. W. L. Smith and H. M. Woolf, November 1974, 13 pp. (COM-75-10432)

NESS 72 An Intercomparison of Radiosonde and Satellite-Derived Cross Sections During the AMTEX. W. C. Shen, W. L. Smith, and H. M. Woolf, February 1975, 18 pp. (COM-75-10439/AS)

NESS 73 Evaluation of a Balanced 300-mb Height Analysis as a Reference Level for Satellite-Derived soundings. Albert Thomasell, Jr., December 1975, 25 pp. (PB-253-058)

NESS 74 On the Estimation of Areal Windspeed Distribution in Tropical Cyclones With the Use of Satellite Data. Andrew Timchalk, August 1976, 41 pp. (PB-261-971)

NESS 75 Guide for Designing RF Ground Receiving Stations for TIROS-N. John R. Schneider, December 1976, 126 pp. (PB-262-931)

NESS 76 Determination of the Earth-Atmosphere Radiation Budget from NOAA Satellite Data. Arnold Gruber, November 1977, 31 pp. (PB-279-633)

NESS 77 Wind Analysis by Conditional Relaxation. Albert Thomasell, Jr., January 1979.

NESS 78 Geostationary Operational Environmental Satellite/Data Collection System. July 1979, 86 pp. (PB-301-276)

NESS 79 Error Characteristics of Satellite-Derived Winds. Lester F. Hubert and Albert Thomasell, Jr. June 1979, 44 pp. (PB-300-754)

NESS 80 Calculation of Atmospheric Radiances and Brightness Temperatures in Infrared Window Channels of Satellite Radiometers. Michael P. Weinreb and Michael L. Hill, March 1980, 43 pp. (PB80 208-119)

NESS 81 Improved Algorithm for Calculation of UTM and Geodetic Coordinates. Jeff Dozier, September 1980, 21 pp. (PB81 132680)

NESS 82 The Effect of Precipitation on Microwave Soundings in Low Latitudes. Lester F. Hubert, Norman C. Grody, Andrew Timchalk, and William C. Shen, April 1981, 34 pp. (PB81 225062)

NESS 83 Atmospheric Sounding User's Guide. Adolf Werbowetzki, ed., April 1981, 82 pp. (PB81 230476)

NESS 84 Use of NOAA/AVHRR Visible and Near-Infrared Data for Land Remote Sensing. Stanley R. Schneider, David F. McGinnis Jr., James A. Gatlin, September 1981.

NESS 85 Transmittances for the TIROS Operational Vertical Sounder. M.P. Weinreb, H.E. Fleming, L.M. McMillin, and A.C. Neuendorffer, September 1981.